A DISSERTATION ON

EFFECT OF MARTENSITE ON DEFORMATION BEHAVIOR OF Ti-6Al-4V

Submitted in partial fulfilment of the requirements for the award of the degree of

Master of Technology

in

Metallurgical and Materials Engineering

(With Specialization in Industrial Metallurgy)

Under the Guidance of Dr. K. S. Suresh

by

Devang Gandhi

Enrolment No. : 16544016

DEPARTMENT OF METALLURGICAL AND MATERIAL ENGINEERING

INDIAN INSTITUTE OF TECHNOLOGY ROORKEE

ROORKEE – 247667 (INDIA)

May, 2018

CANDIDATE'S DECLARATION

I hereby declare that the proposed work presented in this dissertation entitled '**Effect of Martensite on Deformation Behavior of Ti-6Al-4V'** in partial fulfillment of the requirements for the award of the degree of **Master of Technology** in '**Metallurgical and Materials Engineering'** with specialization in **Industrial Metallurgy**, submitted in the **Department of Metallurgical and Materials Engineering**, '**Indian Institute of Technology Roorkee'** is an authentic record of my own work carried out during the period from **July 2017** to **May 2018**, under the supervision of **Dr. K. S. Suresh**, Assistant professor, Department of Metallurgical and Material Engineering, Indian Institute of Technology Roorkee.

The matter presented in this dissertation has not been submitted anywhere in any form by me for awarding any degree.

Dated:
Place: Roorkee **(DEVANG GANDHI)**

CERTIFICATE

This is to certify that the above statement made by the candidate is correct to the best of my knowledge and belief.

(Dr. K. S. Suresh)
Assistant Professor
Department of Metallurgical & Materials Engineering
Indian Institute of Technology Roorkee
Roorkee-247667 (INDIA)

Acknowledgements

The satisfaction and euphoria that accompany the successful completion of any task would be incomplete without the mention of people, whose constant guidance and encouragement crowned our efforts with success. It is a pleasant aspect that we have now the opportunity to express our gratitude for all of them.

First and foremost, I would like to thank **Dr. K. S. SURESH** for encouraging me to undertake this dissertation as well as providing me all the necessary guidance, inspirational support throughout this dissertation work and his patience to cultivate research skills in me. I am indebted to him for giving me the freedom to explore newer avenues in research. He has displayed unique tolerance and understanding at every step of progress. His commitment towards students and research will always inspire me. It is my proud privilege to have carried out this dissertation work under his valuable guidance.

I wish to express my sincere thanks to **Dr. Anjan Sil**, Professor and Head of the Department, Metallurgical and Materials Engineering Department, Indian Institute of Technology Roorkee, for his help to carry out this dissertation.

I would like to thanks all Research scholars at IIT Roorkee for supporting me in starting the journey of research . Also I'd like to name Mohit Madavi, my batchmate for his support, Aniruddha Malakar, Harshal Kulkarni, Shashi Mohan Rao and Naga Chaitanya for extending their help whenever it was needed.

I would like to acknowledge all friends for their valuable information share, and developing love and confidence in me throughout the work. I would be grateful to my parents who have hold my back, encouraged and guided in many uncountable situations and for making my presence on this earth after which everything else was possible.

IIT Roorkee

Date: **(DEVANG GANDHI)**

LIST OF FIGURES

LIST OF FIGURES

LIST OF FIGURES

LIST OF TABLES

ABSTRACT

The Ti-6Al-4V alloy is one of the most widely used titanium alloy for its high specific modulus and moderate ductility because of a variety of microstructures (equiaxed, bimodal, lamellar) where a good range of mechanical properties is attained. In order to increase the strength of Ti-6Al-4V, a microstructure having balanced amount of equiaxed as well as lamellar phase is needed. There are conventional ways like ultra-fine grain refinement in order to increase strength as well as ductility. Another method has been proposed in this report using hot deformation along with annealing followed by quenching to incorporate some amount of martensite. Therefore, the present study aims to calculate the best combinations of different fractions of phases to obtain good combination of properties. The project aims to quantify the amount of martensite generated on cooling from different temperatures. The project also aims to study the effect of martensite on the deformation behavior with the help of electron backscatter diffraction (EBSD) and synchrotron x ray diffraction (S-XRD). Thereby, with the proposed quantity of martensite, EBSD analysis and S-XRD results have given insights about the misorientations and texture related information. The EBSD scans for 4 different conditions were taken in order to understand the grain size, aspect ratio, misorientations and axis/angle distribution. The synchrotron results included calculation for lattice strains and the macro strains for two different conditions which in turn proved beneficial to correlate with texture analysis.

Keywords: Martensite,Electron BackScatter Diffraction(EBSD),Synchrotron X Ray Diffraction(S-XRD)

Table of Contents

1.0 INTRODUCTION

1.1 Titanium

Titanium has been widely used in the aerospace industry for the past 50 years, due to the high specific tensile strength, high corrosion resistance, fatigue and crack resistance along with the ability to withstand moderately high temperatures. The main aim of the aerospace industry includes improving efficiency of the products, with main focus on reduction of cost, environmental impact and safety. In order to reduce cost, light-weight construction is a universal requirement and therefore, materials like titanium and aluminium alloys and composites which have a high strength to weight ratio are being used. About half of the production of the world's titanium is used in aerospace industry. Titanium and its alloys are used mainly for airframes and for gas turbine engines [1]. The materials used in aerospace industry mainly include: ~20% steel (multiple shafts), ~35% nickel (turbine stages), ~40% titanium (fan/compressor), ~5% other materials . Titanium alloys are mainly dominating in the aerospace field and will continue to dominate due to its high specific strength and high corrosion resistance, even at high temperature making it a favorable metal to form high temperature alloys [2].

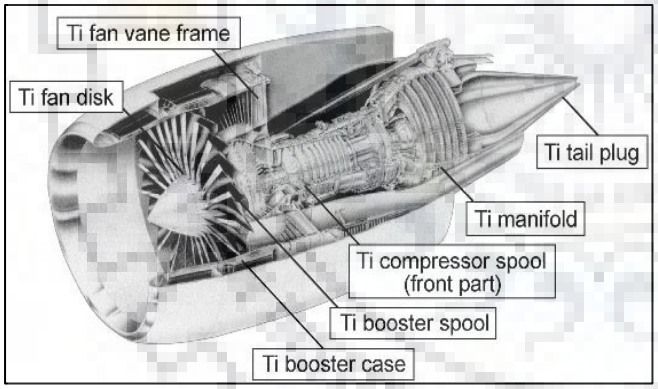

Fig. 1: Ti usage in the GE-90 aero engine [3]

Fig. 2: Ti in bio-medical implants [4]

Apart from the aerospace industry, titanium alloys serves its purpose where good corrosion resistance is required. For this reason, they are mainly used for exposure to sea water. Also, the nature of titanium is bio-compatible and has similar elastic modulus as that of human bone, due to which it is used for medical applications like surgical implants and prostheses. Bone plates, screws, hip nails all have Ti or Ti alloy present in them. The partial and total knee, hip, elbow replacements are produced from unalloyed titanium and Ti-6Al-4V. Thus, Ti alloys are essential and critically used for applications in bio-medical industry.

1.2 Ti-6Al-4V

Ti-6Al-4V is one of the vital Ti alloys and accounts for 60% of all Titanium production. It is undoubtedly called as 'workhorse' of titanium industry. Ti-6Al-4V is an α-β alloy, the alpha phase stabilized by 6 wt% aluminium and the beta phase stabilized by 4 wt% vanadium. At room temperature, the microstructure is mainly α phase (hcp) with some amount of β (bcc). α phase can be stabilized with alloying elements like Al, whereas β can be stabilized with V. The transformation temperature (i.e. β-transus) for Ti-6Al-4V where β↔α takes place lies close to 995° C [5]. The two phases have different crystal structure hence differences in properties. The α phase having lesser slip systems, has higher strength and lower ductility as compared to the β phase which has lower strength but higher ductility.

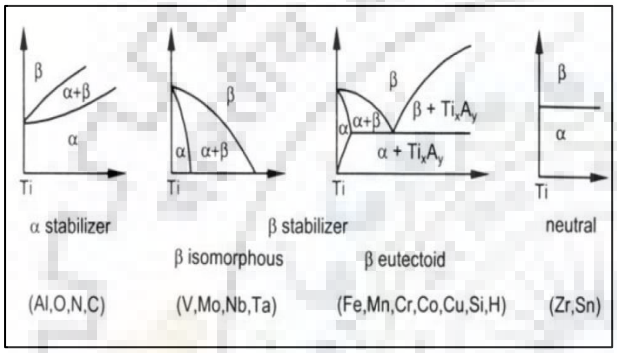

Fig. 3: Phase stability [6]

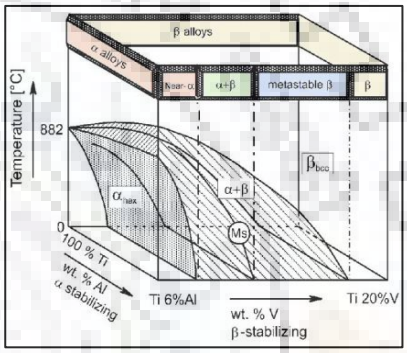

Fig. 4: Ti–Al–V Phase Diagram [5]

Due to the flexibility of the microstructure of Ti-6Al-4V to form fully lamellar or fully equiaxed or bimodal (equiaxed+lamellar) it gives good mechanical properties. The lamellar structure has a better strength than the remaining, whereas the equiaxed possesses a higher amount of ductility. The bimodal structure has good strength as well as good ductility. But, there is always a need to improve strength as well as ductility. There have been ways to increase strength but, those are conventional ways which improve strength at the cost of ductility. Also, there are methods like ultra-fine grain refinement [7] which makes grains refined and thereby, increases strength due to finer grain size, following Hall-Petch relationship. Another method which has been proposed in the following dissertation to improve ductility has been by means of incorporating martensite following deformation in the Ti-6Al-4V alloy. The method proceeds by slow cooling below the β-transus which leads to formation of globular type of α. The formation of martensite in this globular microstructure could enhance the strength of the alloy. The following report includes heat treatment conditions and the effect of the martensite on the deformation behavior of the alloy.

1.3 Effect of deformation and heat treatment on Ti-6Al-4V

The mechanical properties on an alloy depends on the phases present in the alloy. Ti-6Al-4V is supposedly to have a two phase microstructure consisting of hexagonal close packed (hcp) α and body centred cubic (bcc) β as equilibrium microstructures. The two phases are stable are at room temperature for Ti-6Al-4V and above the β transus, only β phase is stable. Depending on the amount of phases, the material will behave accordingly. For e.g. the α phase being h.c.p will have lower ductility but higher strength, whereas β phase will give higher ductility due to more number of slip systems. Also, for the occurrence of a particular phase, it could be by dynamic means e.g. thermo-mechanical processing or by static heat treatment in order to achieve better mechanical properties.

The thermo-mechanical processing condition may be above β region or in the α+β region. Depending on the morphology of grain and phases required it is important to decide the processing temperature. Deformation like forging above beta transus leads to coarse grained microstructure leading to loss of mechanical properties like strength and ductility. In the α+β region, if transformation is done, there is transformation of morphology of α. This transformation of α is different from that of primary α. The prior β grains transform to co-oriented lamellae of α (transformed α) which are separated by rib like features of retained β phase [8]. The relative amount of primary α and transformed β gives significant changes in strength and ductility of the material. Hence, it is noteworthy to use this property of α in order to obtain morphology of grains as per the application of the alloy.

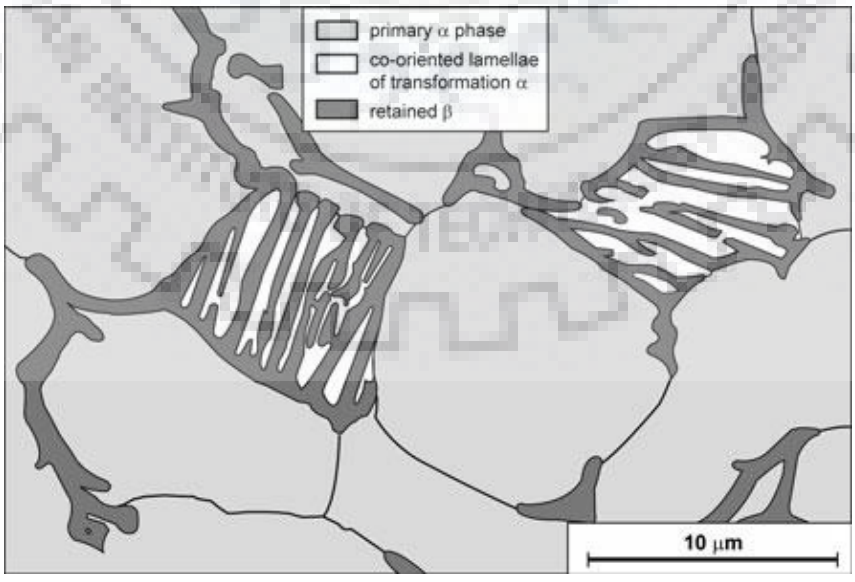

Fig. 5: Graphical Representation of β to Transformed α [8]

1.4 Role of Martensite on strength and ductility in Ti-6Al-4V

The deformation of Titanium alloys is more complex than that of cubic materials. It is the h.c.p crystal which makes the deformation harder in Ti alloys. The hot deformation involves recrystallization and globularization of the α phase. Extensive literature is available on techniques and mechanism to generate equiaxed microstructure via deformation processes like forging, hot rolling and stamping for different Ti alloys [9] [10]. The equiaxed microstructure along with fractions of martensite can help in improving strength as well as ductility in the alloy. The martensite can be formed by quenching the sample from the β phase region or α+β region to a temperature below M_s temperature.

The martensite in Ti-6Al-4V plays a crucial role in increasing the strength of the alloy. During deformation, stress induced martensites (SIM) are being produced which helps in increasing the strength of the alloy. The deformation induces the β phase to transforme to fine α′ martensites. The role of these martensites in increasing strength has been explained from the tensile tests performed by Matsumoto et al. [11], in various heat treat conditions of alpha-beta (1223K) and beta (1373K) regime with cooling rate as water quenched (STQ)and furnace cooled (ST-FC) .

Another example where rolling of Ti-6Al-4V sheets were done and then heat treated and water quenched was done by Fan et al. [12]. The range of temperatures used was 650°C to 1050°C. The results suggested using an acicular α′ martensitic structure for high 0.2% proof stress whereas equiaxed microstructure for ductility of the hot-tolled sheet sample.

Microstructure	0.2% proof stress		Elongation	
	(MPa)	(Δ%)	(%)	(Δ%)
As-received (equiaxed grain size = 15–20 μm)	978	0	13.6	0
Bimodal (950A) (equiaxed grain size = 15–20 μm + lamellar width of 2–4 μm)	1017	4.00	11.8	–13.6
Widmanstätten (1050A) (lamellar width of 10 μm + >400 μm α grain boundary)	1041	6.42	10.3	–24.4
Martensite (1050Q) (200 μm grain size with inside acicular α′)	1114	13.8	7.8	–42.7

Fig. 6: Tensile Test result from literature for various morphology [12]

2.0 LITERATURE SURVEY

2.1 Deformation modes in HCP phase

There are mainly two modes of deformation in titanium alloys. Those are the slip and twinning. Titanium has many slip planes and slip directions. In the α form, it has a c/a ratio of 1.586 which is less than the ideal value of 1.633 for HCP. Thus, it is intrinsically strongly anisotropic. The active slip planes include the basal (0002) planes, the prismatic planes of {10-10} family and pyramidal planes of {10-11} family. The planes consist of three closed packed direction of type <11-20>, the main slip direction. The planes along with possible slip directions give rise to 12 slip systems in total. But there are two slip systems whose combined action duplicates the action of other slip systems. Hence, there are only 4 independent slip systems.

The ease of plastic deformation increases from the hexagonal closed packed (hcp) to body centered cubic (bcc). The presence of only 3 slip system makes it difficult for the deformation. As per the Von Mises criterion for homogenous plastic deformation of polycrystals, there must be 5 active slip systems. Hence in order to have plastic deformation <c+a> slip or twinning must be activated. For α+β titanium alloys like Ti-6Al-4V, twinning has been suppressed for Al > 5 wt %, <c+a> slip is chosen for plastic deformation along c axis.

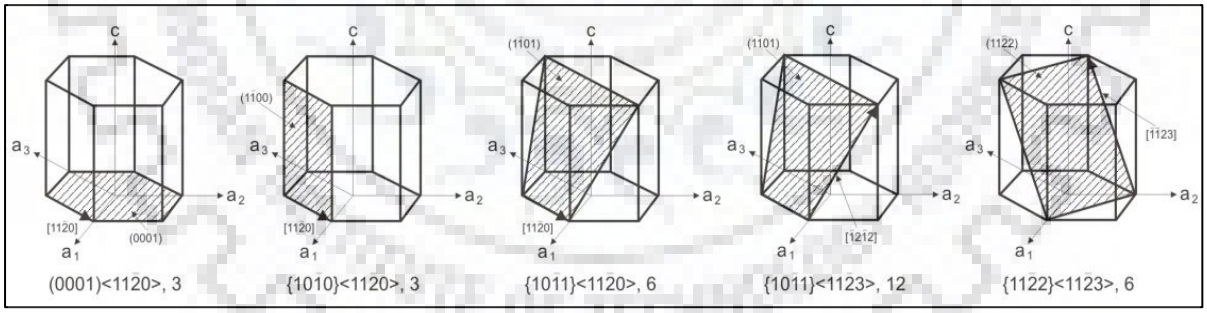

Fig. 7: Slip systems in α titanium [5]

There are various twinning modes that are prevalent in Ti alloys. The main ones include {10-12}, {11-21}, {11-22} planes. The twins that occurs on the {11-21} planes are known as as extension or tensile twins since they involve a tensile stress along the c axis and while the twins that forms on the {11-22} planes are called as contraction twins, since this involves a compressive stress along c axis. Twinning is mainly dependent on the applied stress direction.

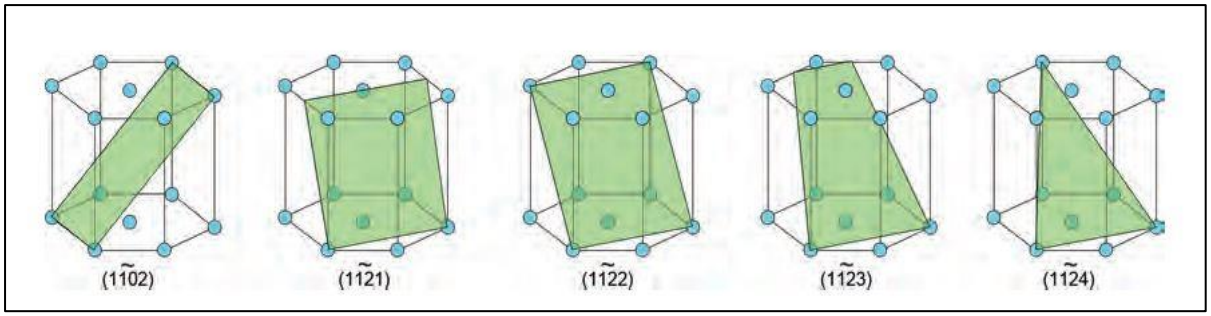

Fig. 8: Twinning planes in titanium alloys [5]

Apart from α and β phase, there may be presence of a metastable phase, which is of martensite. In Titanium alloys, the martensites are of two types : α′ and α″. The hexagonal type α′ martensite is a result of shear transformation in [111]$_\beta$ (112)$_\beta$ and [111]$_\beta$ (-101)$_\beta$ or in hexagonal notation: [2-1-13]$_\alpha$ (2-1-12)$_\alpha$ and [2-1-13]$_\alpha$ (-1011)$_\alpha$ [3]. The morphologies of martensite of α′ can be massive or acicular. Generally, massive martensites are obtained in pure Ti or very dilute alloys whereas acicular martensites are obtained in high alloy Ti system, and consist of mixture of individual α plates, with a different variant of the Burger relationship.

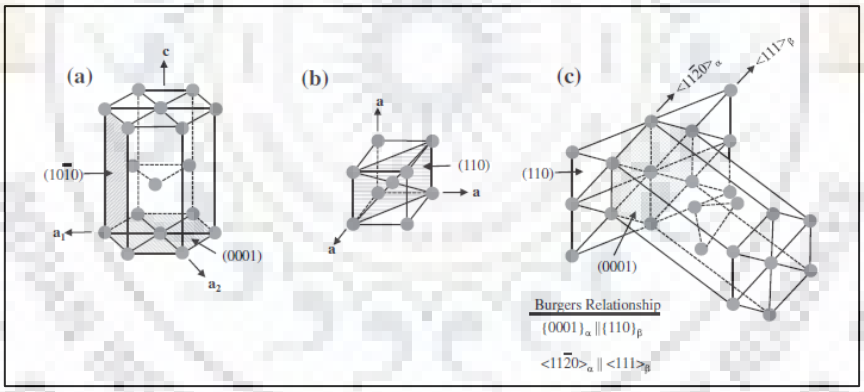

Fig. 9: The phases of Ti-6Al-4V (a) H.C.P. α (b) B.C.C. β (c) Hexagonal α′ [13]

The orthorhombic martensite is formed in high solute content of Ti alloy as α″, when the hexagonal structure becomes distorted and becomes orthorhombic. An example of one such instance is when the β phase is quenched with vanadium content in range of 10%-12%, from temperatures between, 750°C-900°C the soft orthorhombic phase α″ tends to form along with the β phase [14]. Apart from the martensites, another athermal phase ω is also present in titanium alloys. This occurs when the β phase decomposes upon quenching in an athermal manner so as to form the ω phase. The ω phase has a trigonal symmetry in case of heavily stabilized β alloys and hexagonal in case of leaner Ti alloys. The ω phase can be suppressed by aging the sample at temperatures (in range of 500°C-600°C) [3].

2.2 Globularization via Hot Deformation

During the hot deformation of the Ti-6Al-4V alloy, recrystallization of the microstructure occurs, provided deformation temperature and plastic strain are sufficient. The recrystallization that is achieved during deformation is known as dynamic re-crystallization (DRX). The dynamic re-crystallization is of two types: discontinuous dynamic re-crystallization (DDRX) and continuous dynamic re-crystallization (CDRX).

1. DDRX : New grains formed by heterogeneous nucleation and growth. Two step process, nucleation of new dislocation-free grain with high angle grain boundaries followed by long distance migration.

2. CDRX : Sub-grains with low-angle boundaries formed, evolve into grains with high fraction of high angle boundaries, increase in plastic strain. One step process is nucleation of new grains with dislocations distributed in homogenous way.

Combined with globularization, DRX leads to the formation of equiaxed grain morphology. The process of creating an equiaxed α morphology from needles/platelets is known as globularization (spheroidization, general term). The globularization of Ti-6Al-4V during thermo-mechanical processing takes place by 2 ways :

1. Fault Migration / Termination Migration : The fault migration also known as termination migration is dependent on diffusion, and the driving force responsible for this is the gradient in chemical potential between the interphase boundary of the platelet and the curved edge of the platelet. The solute atoms diffuse from the edge to the flat surface, creating coarsening of the platelet or globularization of the individual lamellae. In α+β alloys, the kinetics of globularization depends on the energy at the interphase boundaries [15].

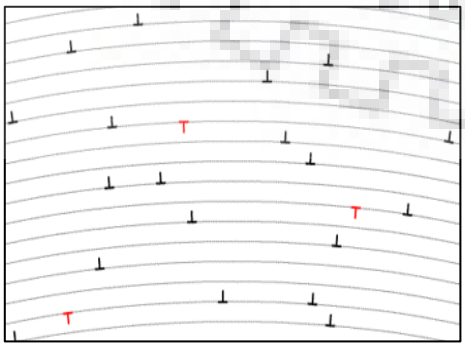

Fig. 10: Fault Migration

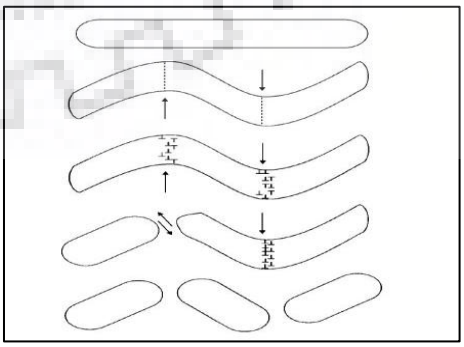

Fig. 11: Formation of Kinks [16]

2. Fragmentation of lamellae : The fragmentation of lamellae takes place by three steps. Initially, there is kink formation of the plates and the frequency is proportional to the strain applied. The colonies of α orient themselves favorably with respect to stress applied and form kinks, whereas remaining colonies orient to form further kinking. The dislocations of both +/- signs are formed along the shear line at the preferred kink point. Annihilation of these opposite sign dislocations takes place resulting in accumulation of remaining dislocations. The energy therefore, is increased at the kinked interface. To reduce this interfacial energy, globules are formed by surface migration. Thus, obtaining an equiaxed microstructure with fine grains along with high dislocation density, close to grain boundary region. [16]

In multiple journal papers, various scientists have worked with globularization and with different deformation mechanisms. The globularization during the multiple forging at temperatures of 700°C to 950°C was studied by Digvijay et al. [9] where the mechanism of globularization by means of breaking of the initial α colony structure was studied. Another instance of study of globularization during hot rolling was done by Syed et al. [10] where the effect of the rolling temperature on the spheroidization of a near-alpha Ti alloy was studied. Zhang et al. [17] performed deformation at temperatures of 800° C and 850° C at low strain rates to generate equiaxed grains from a bimodal starting microstructure. Abbasi and Momeni [18] worked on the deformation behaviour of Ti-6Al-4V with compression tests as well as hot rolling at temperature range of 820° C -1070° C. The rolling in α/β phase on cooling generated a partially globularized structure whereas rolling in the β phase field gave rise to martensite upon cooling. Also, it was mentioned that the minimum temperature and minimum strain required for dynamic globularization to take place was 850°C and 2 respectively.

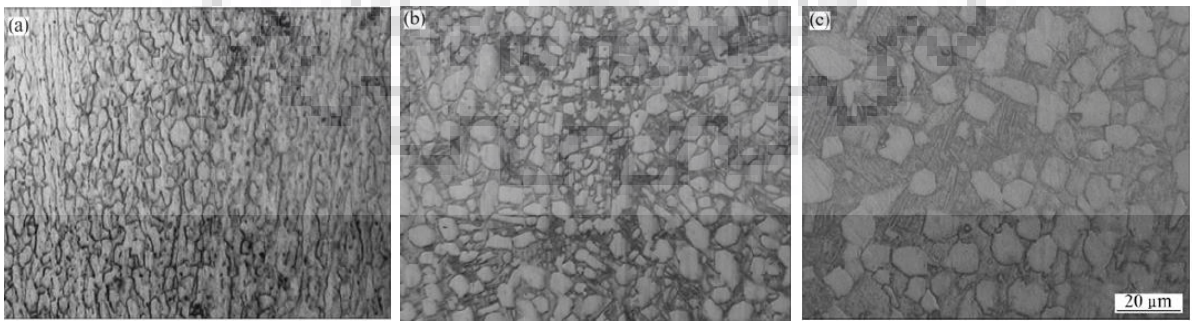

Fig. 12: Globularization (at 920°C, 2hours) post hot rolling at temperatures

(a) 820°C (b) 870°C (c) 920°C [18]

2.3 Introducing Martensite in Titanium Alloys

The most common type of martensite found in Ti-6Al-4V is the hexagonal type α' martensite. It occurs as colonies of parallel side plate or in form of laths. The internal region of this martensite is heavily dislocated. The martensitic start temperature for Ti-6AL-4V alloy is around 880°C. With higher content of solute, the M_s temperature decreases and the size of these colonies decrease and they obtain a lenticular or acicular morphology. The orientation relationship of this α' martensite with the β phase is as follows: $(0001)_{\alpha'} // (110)_{\beta}$, $[11\text{-}20]_{\alpha'} // [111]_{\beta}$.

Table 1: Types of Martensite

Type	Crystal Structure	Examples	Orientation Relationship
α'	Hexagonal	Ti-6Al-4V	$(110)_{\beta} // (0001)_{\alpha'}$, $[111]_{\beta} // [11\text{-}20]_{\alpha'}$
α''	Orthorhombic	Ti-6Al-2Sn-4Zr-6Mo	$(011)_{\beta} // (001)_{\alpha''}$, $[111]_{\beta} // [110]_{\alpha''}$

The other type of martensite found in these alloys is the orthorhombic type α'' martensite. It occurs mainly due to transformation from hexagonal α' to orthorhombic α'' and is found in alloys with higher solute content. Its presence lowers the ductility of Ti alloys that leads to poor formability. Therefore it should be avoided in titanium alloys designed for structural applications.

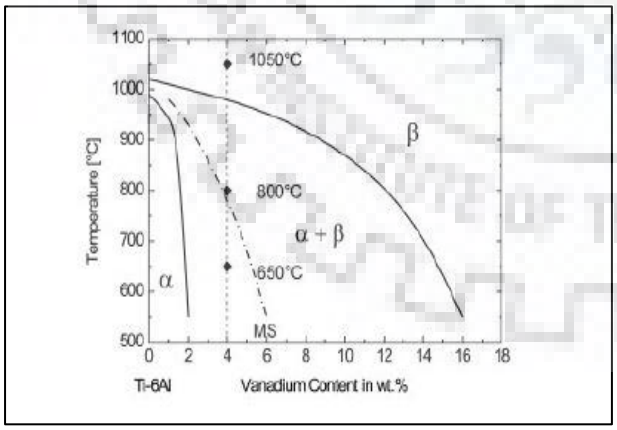

Fig. 13: Representation of M_s Temperature

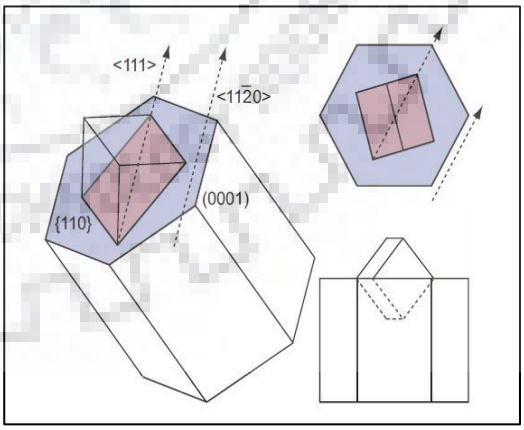

Fig. 14: Phase Transformation β↔α′ [5]

The martensitic phase transformation in Ti-6Al-4V occurs from β phase. From a particular β orientation, there can be 12 possible combinations of α that could form during phase transformation. In case of Steels, there are martensitic transformations in which certain

orientations (or variants) occur more often than other orientations [19]. The phenomenon is known as variant selection. For Ti-6Al-4V the 12 variants and their Burger orientation relationship relating the β phase to α phase.

Twelve possible variants generated by the martensitic β → α phase transformation through the Burgers orientation relationship

Variant	Plane parallel	Direction parallel	Rotation angle/axis from V1
V1	$(1\,\bar{1}\,0)_\beta \parallel (0\,0\,0\,1)_\alpha$	$[1\,1\,1]_\beta \parallel [1\,1\,\bar{2}\,0]_\alpha$	–
V2	$(1\,0\,\bar{1})_\beta \parallel (0\,0\,0\,1)_\alpha$	$[1\,1\,1]_\beta \parallel [1\,1\,\bar{2}\,0]_\alpha$	60°/[1 1 $\bar{2}$ 0]
V3	$(0\,1\,\bar{1})_\beta \parallel (0\,0\,0\,1)_\alpha$	$[1\,1\,1]_\beta \parallel [1\,1\,\bar{2}\,0]_\alpha$	60°/[1 1 $\bar{2}$ 0]
V4	$(1\,1\,0)_\beta \parallel (0\,0\,0\,1)_\alpha$	$[\bar{1}\,1\,1]_\beta \parallel [1\,1\,\bar{2}\,0]_\alpha$	90°/[1 $\overline{2.38}$ 1.38 0]
V5	$(1\,0\,1)_\beta \parallel (0\,0\,0\,1)_\alpha$	$[\bar{1}\,1\,1]_\beta \parallel [1\,1\,\bar{2}\,0]_\alpha$	63.26°/[$\bar{1}\bar{0}$ 5 5 $\bar{3}$]
V6	$(0\,1\,\bar{1})_\beta \parallel (0\,0\,0\,1)_\alpha$	$[\bar{1}\,1\,1]_\beta \parallel [1\,1\,\bar{2}\,0]_\alpha$	60.83°/[$\overline{1.377}$ 1 2.377 0.359]
V7	$(1\,1\,0)_\beta \parallel (0\,0\,0\,1)_\alpha$	$[1\,\bar{1}\,1]_\beta \parallel [1\,1\,\bar{2}\,0]_\alpha$	90°/[1 $\overline{2.38}$ 1.38 0]
V8	$(1\,0\,\bar{1})_\beta \parallel (0\,0\,0\,1)_\alpha$	$[1\,\bar{1}\,1]_\beta \parallel [1\,1\,\bar{2}\,0]_\alpha$	60.83°/[$\overline{1.377}$ 1 2.377 0.359]
V9	$(0\,1\,1)_\beta \parallel (0\,0\,0\,1)_\alpha$	$[1\,\bar{1}\,1]_\beta \parallel [1\,1\,\bar{2}\,0]_\alpha$	63.26°/[$\bar{1}\bar{0}$ 5 5 $\bar{3}$]
V10	$(1\,\bar{1}\,0)_\beta \parallel (0\,0\,0\,1)_\alpha$	$[1\,1\,\bar{1}]_\beta \parallel [1\,1\,\bar{2}\,0]_\alpha$	10.53°/[0001]
V11	$(1\,0\,1)_\beta \parallel (0\,0\,0\,1)_\alpha$	$[1\,1\,\bar{1}]_\beta \parallel [1\,1\,\bar{2}\,0]_\alpha$	60.83°/[$\overline{1.377}$ 1 2.377 0.359]
V12	$(0\,1\,1)_\beta \parallel (0\,0\,0\,1)_\alpha$	$[1\,1\,\bar{1}]_\beta \parallel [1\,1\,\bar{2}\,0]_\alpha$	60.83°/[$\overline{1.377}$ 1 2.377 0.359]

Fig. 15: 12 Variants of α′ Martensite [13]

Depending on the various parameters of annealing temperature and cooling rate, the extent of variant selection can be found by using electron back scatter diffraction. The cooling rate and combination of temperature may/may not give rise to martensitic microstructure. Above the Ms temperature, the lamellar and equiaxed morphology is obtained in microstructure whereas below the Ms temperature, the microstructure is only equiaxed. The study of these microstructures could be done using back scatter electron imaging and electron back scatter diffraction.

2.4 Characterization of Martensite

The Electron Back-Scatter Diffraction (EBSD) is used to observe the local and bulk misorientation developed in the hot deformed heat treated Ti-6Al-4V alloy. The study of martensite on the deformation behavior of Ti-6Al-4V sample was done using EBSD by Beladi et al. [13]. The study of EBSD provides with various aspects of a sample like inverse pole figures, misorientation angles, grain size, aspect ratio, orientation spread and bulk texture. Various scientists have worked with Ti-6Al-4V samples to characterize the phase as equiaxed or lamellar depending on the misorienation angle [13] [20]. The misorientation angle as defined by A. D. Rollett is transformation required to transform tensor quantities from one set of crystal axes to the other set. Along with the characterization of phases, it is also possible to know the rotation angle of one plane with respect to another via the plot obtained for misorientation angle and axis/angle distribution. This has been studied in detail so as to characterize for texture related components of the sample.

The IPF Maps for the α Ti sample are shown in Fig. 16 containing mostly lamellar phase and equiaxed phase. The distribution for the misorientation angles of the EBSD scan (Fig. 16B) is calculated by Wang et al. [20] is shown in Fig. 17B.

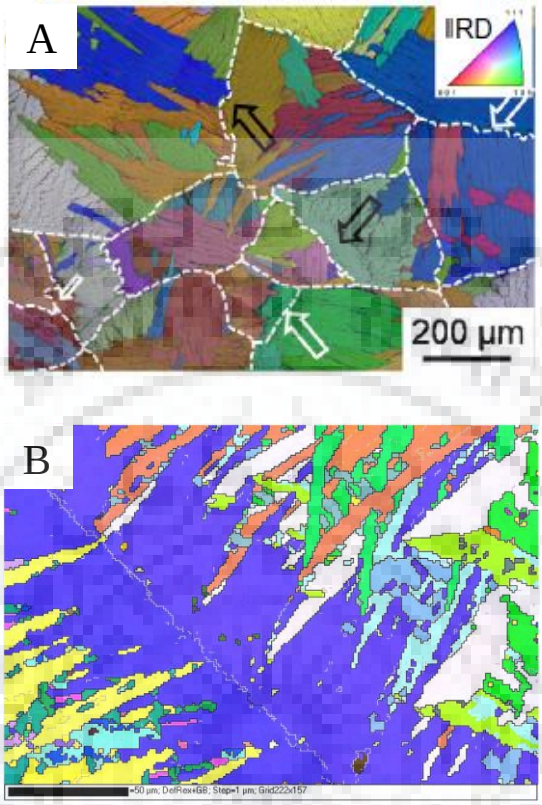

Fig. 16: EBSD scan for Lamellar phase in Ti-6Al-4V (A) [13] (B) [20]

The plots for misorientations as shown in Fig. 17 showed five major misorientations at the following angles of 10º, 60º, 60.83º, 63.26º and 90º. These misorientations were from 12 Burger relationship and shows the dominance of one variant over one another.

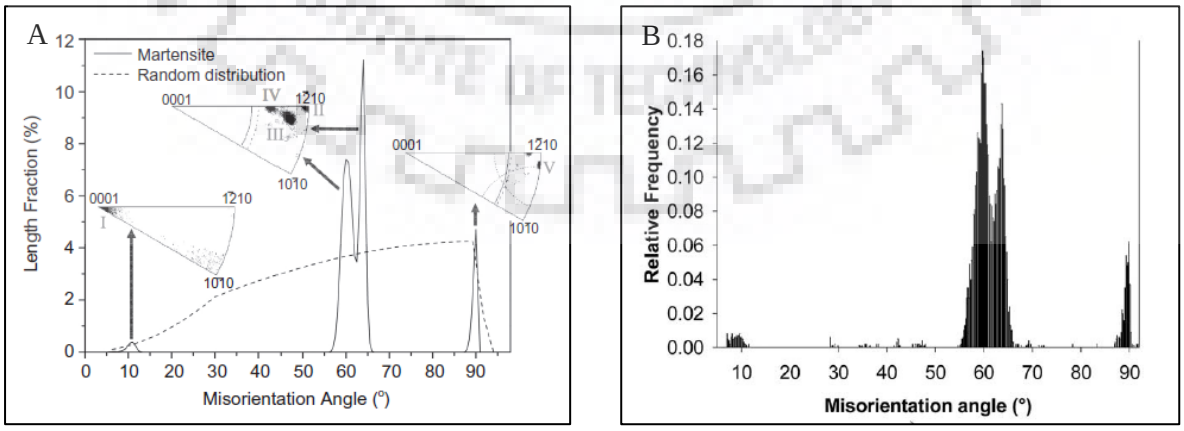

Fig. 17: Misorientation Angle for Lamellar Phase as (a) in EBSD Fig. 16 (A) [13] and in (B) as in EBSD Fig. 16 (b). [20]

2.5 Influence of Martensite on Mechanical Properties

Matsumoto et al. [11] performed several tensile tests with the as received, hot rolled and heat treated samples. The tensile results showed the increase in ductility when heat treated in α+ β phase, whereas the ductility decreased drastically when the sample was treated above the β transus region. The microstructure of those samples explains the reason for the ductility and strength combination.

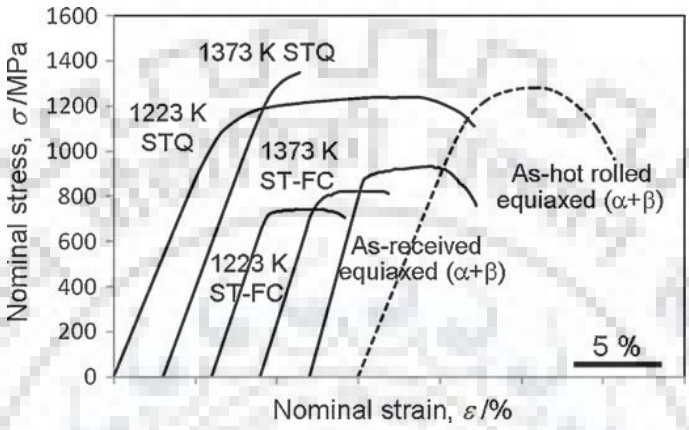

Fig. 18: Tensile tests after hot rolling and heat treatment [11]

The microstructure for the samples from the same paper Matsumoto [11] is given as follows. These were responsible for the strength of the Ti-6Al-4V alloy. The presence of equiaxed as well as lamellar structure in below β transus region and quenching to form martensite helped in having strength as well as ductility.

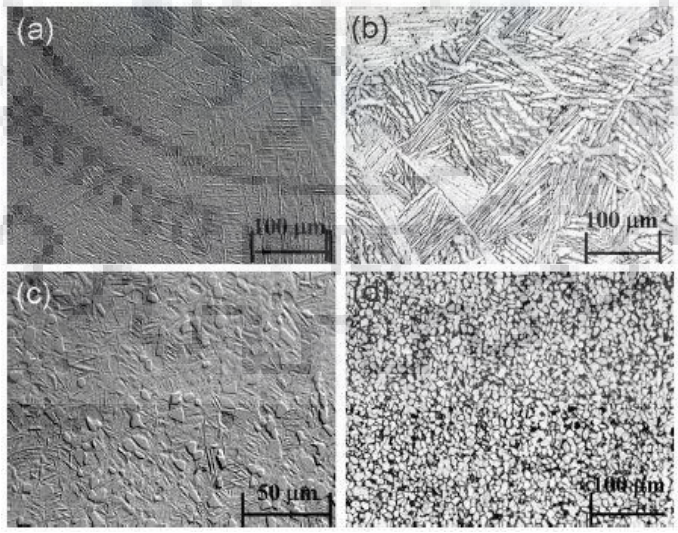

Fig. 19: Micrographs for Samples from Matsumoto et al. [11]
(a) 1100° C STQ (b) 1100° C STFC (c) 950° C STQ (d) 950° C STFC

Following the tensile test, the samples were characterized by synchrotron diffraction. The synchrotron X ray diffraction is done mainly to obtain better statistical information combined with high resolution as compared to normal powder X ray diffraction. This is mainly because of the high energy and great intensity of the beam generated in the synchrotron. It has better counting statistics due to the intensity of beam which in turn leads to more intense peaks and better signal noise ratio. A significance low angle peak broadening found in X Ray Diffractometer is also reduced for the Synchrotron X Ray Diffraction. The in-situ deformations are best studied with S-XRD due to the high spatial resolution, high data collection speed and high sample penetration which allows it to study the deformation in real time. The high energy X rays being produced in synchrotron are used to obtain quantitative information on the different orientation and their response to stress, i.e. phase transformation under external loads.

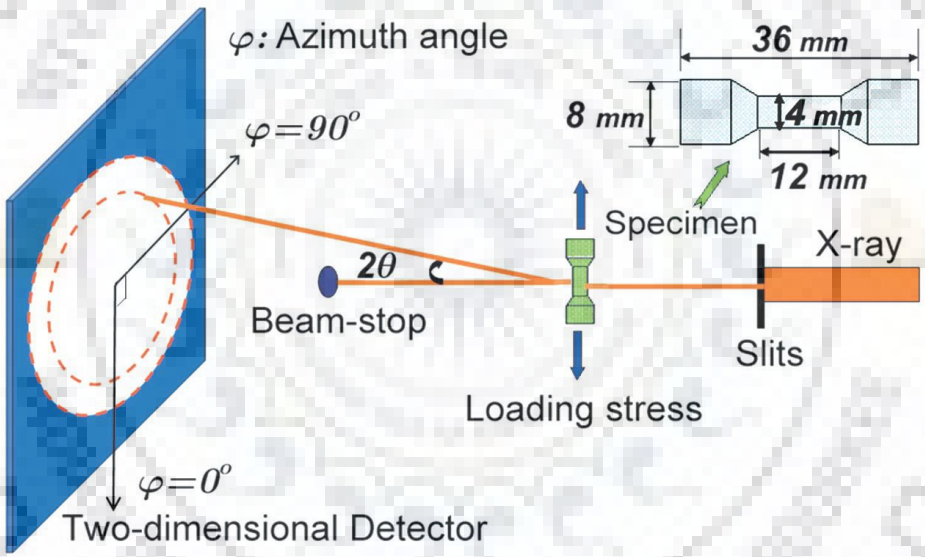

Fig. 20: Synchrotron X Ray Diffraction [21]

The martensites present in the sample are transformed from the β phase to α′. The peaks of α and α′ are difficult to separate the main peaks belonging to α and α′ under the conventional X ray diffraction. Hence there is a need to study the effect of martensites with the help of Synchrotron X Ray Diffraction (S-XRD). The limitations of conventional XRD are overcome with the use of shorter wavelength and better monochromaticity in S-XRD. Apart from the Synchrotron, the mechanical properties studied for martensite include difference in mechanical properties like Young's modulus or the nano-hardness.

The equiaxed and lamellar morphologies along with various parameters like morphology, misorientation angle and strength have difference in nano-hardness too. The use of nano-indentations to find nano-hardness and Young's modulus for different phases is carried out. The values for Young's modulus of β phase (E_β) from a formula given by Elfer et al. for Ti-6Al-4V turns out to be 80.9 GPa [22]. The values for the Young's modulus of the α phase were measured using atomic force acoustic microscopy which obtained values between 120-145 GPa for the α phase. The 4 planes of α had different values i.e. 121.1 GPa for (100) and (110) plane, 142.7 GPa for (001) plane and 130.3 GPa for (101) plane [23] as in Fig. 21.

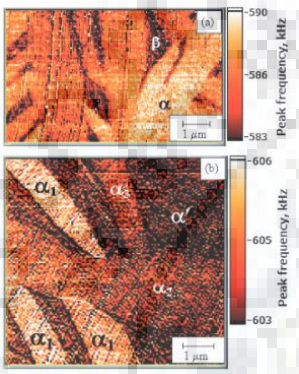

α Plane	Indentation Modulus
$\alpha_1 \rightarrow$ (001)	142.7 GPa
$\alpha_2 \rightarrow$ (101)	130.3 GPa
$\alpha_3 \rightarrow$ (100), (110)	121.1 GPa

Fig. 21: Young's Modulus values for 3 different planes of α phase [23]

The nano-hardness for the Ti-6Al-4V would depend on the morphology of the sample which would depend on the quenching temperature. Jun et al. quenched the Ti-6Al-4V alloys in the α+β region and took micronindentations to obtain the change in hardness with respect to indenter displacement and the quenching temperature. The following are the micrographs with the correspong obtained hardness and Young's modulus values [24].

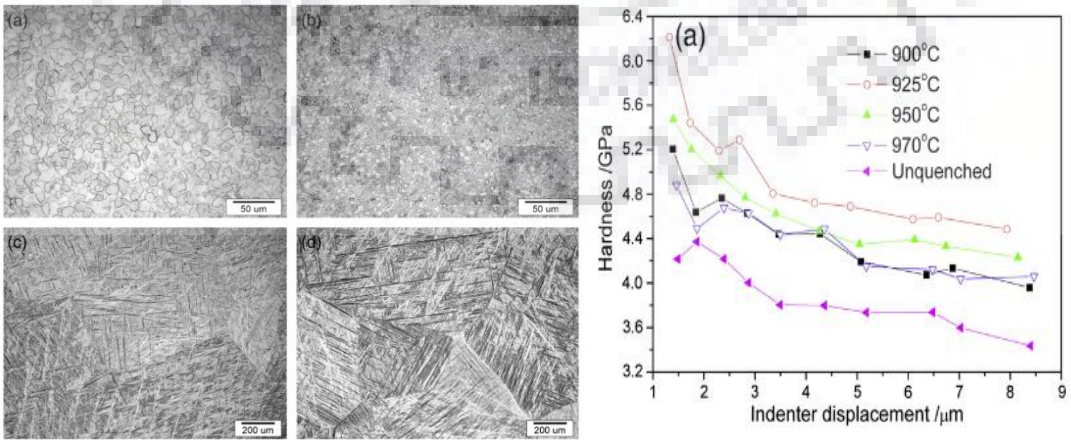

Fig. 22: Nano-Hardness values with respect to different quenching temperatures [24]

3.0 AIM AND OBJECTIVE

3.1 Aim

Although Ti alloys are being widely used in many applications including biomedical and aerospace industries, an enhancement in terms of its specific strength and ductility is still warranted. Earlier investigations on the incorporations of martensite has shown a large enhancement in strength but with a drastic decrease in ductility, the recent investigations described in work done by Matsumoto et al. [11], demonstrates simultaneous enhancement in both the strength and ductility, for materials with controlled presence of martensite. However, there is no agreement on the required amount of martensite for the best combinations of strength and ductility and further the mechanisms of deformation leading to higher ductility is also not known. Therefore, the present study aims to calculate the best combinations of different fractions of phases to obtain good combination of strength and ductility. The project aims to quantify the amount of martensite generated on cooling from different temperatures. Thereby, with the proposed quantity of martensite, results from tensile tests will be used to understand the deformation behavior. The EBSD analysis were performed on selected samples. Thus, it helped in understaning of morphology, size distribution and misorientations of the grains.

3.2 Objective

The objective of the project work is to generate martensite along with equiaxed morphology in order to achieve good mechanical properties like strength and ductility. With the equiaxed phase, being essential for the ductility of Ti-6Al-4V, generation of some volume fraction of martensite improves strength as well as ductility. The objective therefore lies to generate different fractions of martensite and co-relate the properties with the microstructure.

3.3 Plan of Work

The plan of work as per Fig. 23 is shown as below in following sequence :

- Hot Rolling at temperature of 750° C to reduce thickness from 7 mm to 2 mm keeping the strain in range of 0.15 to 0.21.
- Post Deformation Heat Treatment given at 850° C for 1 hour to ensure globularization of Ti-6Al-4V sheet.
- In order to generate Martensite in Globularized α, specimen were heat treated to temperatures of 880° C, 890° C, 900° C, 925° C, 950° C for 30 minutes and water quenched.
- Quantitative morphology analysis (equiaxed and lamellar) by ImageJ software of SEM images along with XRD Results.
- Electron Back Scatter Diffraction of Samples to observe the microstructure and morphology of grains along with grain size, aspect ratio and misorientation angle.
- Evaluation of Mechanical Properties by Tensile Testing of the Specimens along with Synchrotron X Ray Diffraction.
- Fractography and near-fracture cross-section microstructure to check for Deformation-Induced Martensites (DIM).

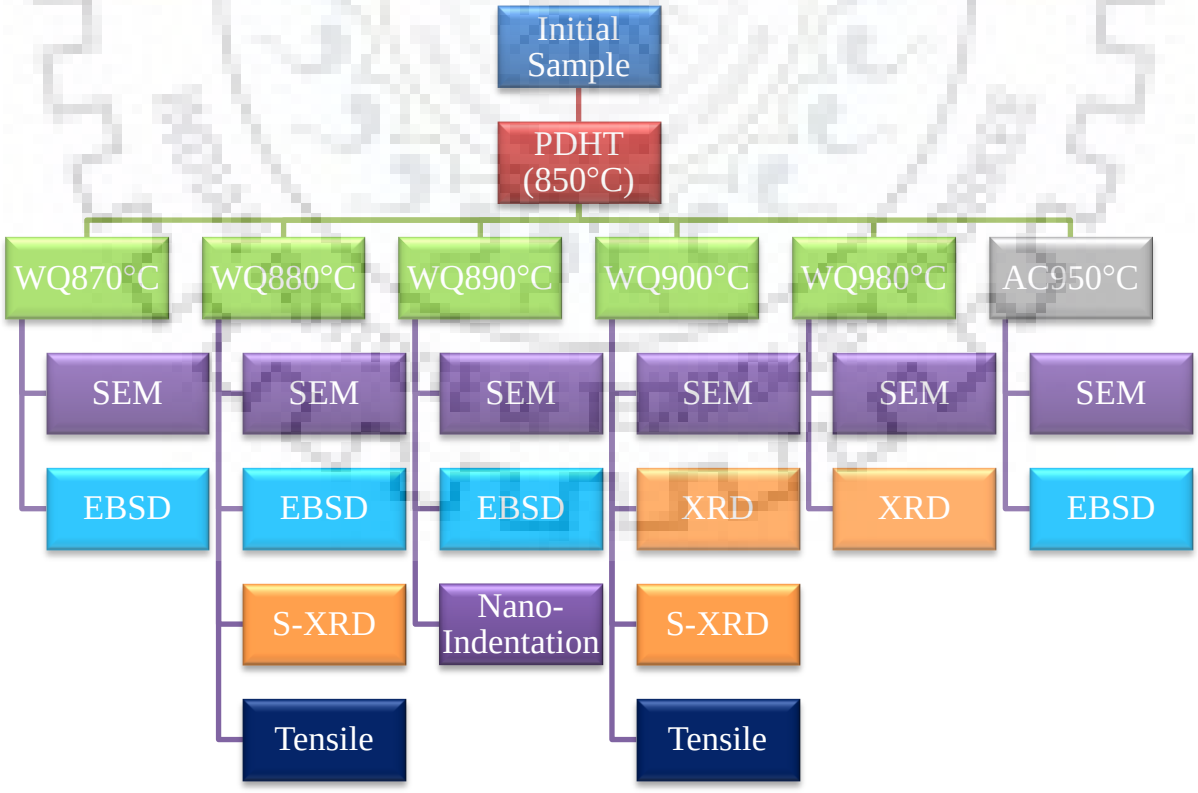

Fig. 23: Plan of Work

4.0 EXPERIMENTAL PROCEDURE

4.1 Material and Methods

The Ti-6Al-4V sample was received in the form of a plate having dimensions as follows : 150 mm × 150 mm × 7 mm. The as-received sample was characterized for metallography, micro-hardness, X-ray diffraction and Thermo-Gravimetric Analysis /Differential Thermal Analysis. The composition analysis of the sample was done using Energy Dispersive Spectroscopy (Fig. 24 and Table 2).

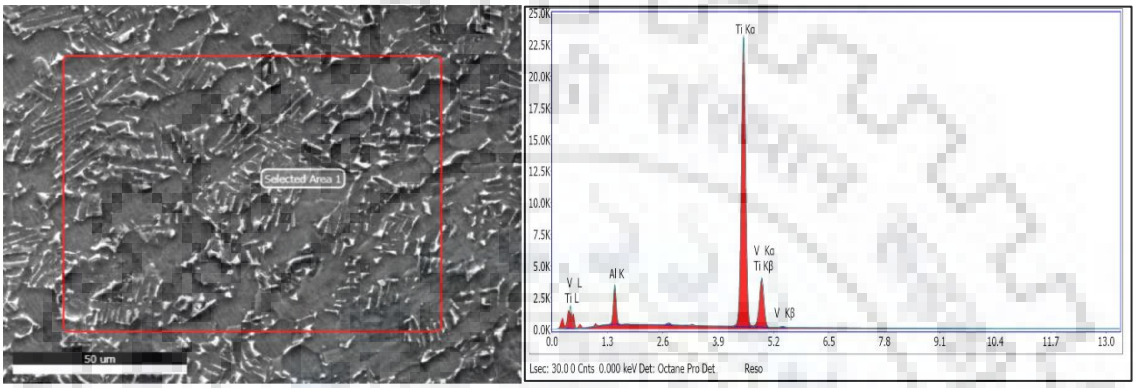

Fig. 24: Composition analysis from Energy Dispersive Spectroscopy (EDS)

Table 2: Composition of Ti-6Al-4V Sample

Element	Ti (%)	Al (%)	V (%)
Weight (%)	89.23	6.23	4.54

The microstructure for the as-received sample was determined after following the conventional metallographic polishing techniques for the sample. Grinding followed by emery paper polishing, followed by cloth polishing and electro-polishing was used to generate a scratch-free surface. Electro-polishing was performed using an electrolyte of 600 ml of ethanol, 360 ml of butoxy-ethanol and 60 ml of perchloric acid. The parameters selected for electro-polishing were 32 V for 50 seconds at 5°C. The samples were then observed under scanning electron microscope to get the micrographs (Fig. 25). The microstructural evolution for the sample revealed the Ti-6Al-4V alloy to be bimodal in nature. The sample had lamellae as well as globular morphology. Following SEM images, quantification for phases was done using ImageJ analysis software. The volume fractions of the lamellar and the equiaxed morphologies are shown in Table 3.

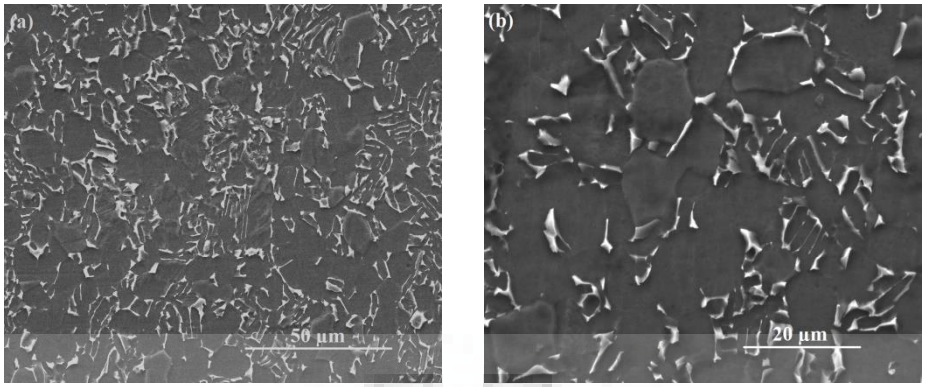

µµFig. 25: SEM Images of initial Ti-6Al-4V at different magnifications µ

(a) 1000X (b) 2000X

Table 3: Initial Sample Morphology Distribution

Morphology of As-Received Sample	Avg. Area (µm^2)	Number of Grains	Total Area (µm^2)	(Phase Fraction %)
Equiaxed	200	87	17400	43.07 %
Lamellar	600	46	27600	56.93 %

The micro-hardness for the sample was done using Vickers Microhardness Tester. The value obtained was 395 VHN. The examination of the TGA results show that the heating of the Ti-6Al-4V (at the heating rate of 20° C/min) in presence of Argon atmosphere showed change in weight at 987° C which is the transformation temperature from β↔α (i.e. β transus). The X-ray diffraction using Cobalt as the source was performed on the initial sample to resolve the peaks for the phases present.

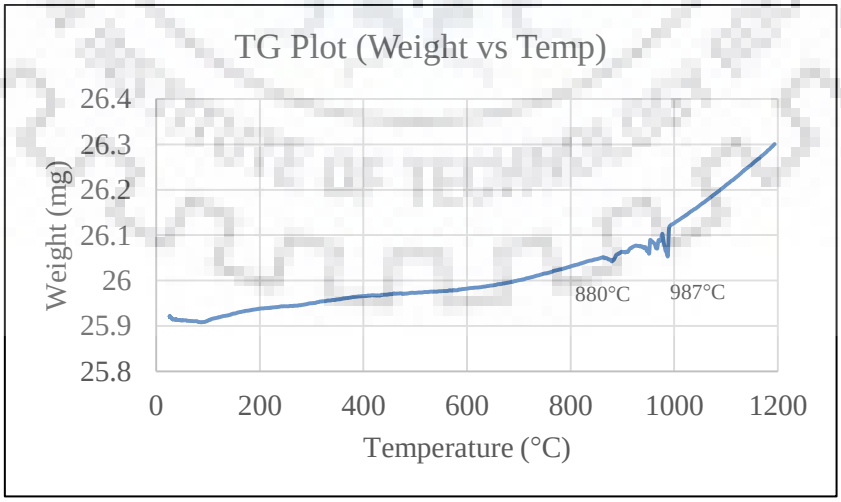

Fig. 26: Thermo-Gravimetric Analysis of initial Ti-6Al-4V

The peaks were indexed for the set of reflections for hexagonal using the formula of interplanar spacing d and hkl set of reflections from the given formula where a and c are the lattice parameters for the α phase of Titanium.

$$\frac{1}{d^2} = \frac{h^2 + k^2}{a^2} + \frac{l^2}{c^2}$$

The following were peaks obtained and analysed for As-Received sample as shown in Fig. 27 and Table 4.

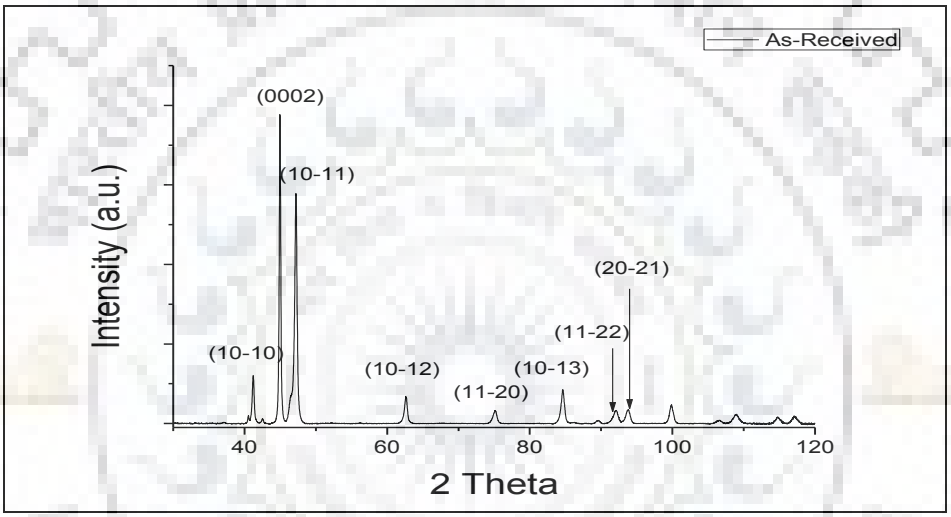

Fig. 27: XRD Analysis of Initial Ti-6Al-4V

Table 4: Identification of hkil planes from XRD

2θ	d= λ/(2 sin θ)	hkl	hkil
41.223	2.5422	(100)	(10-10)
44.976	2.3397	(002)	(0002)
47.232	2.2340	(101)	(10-11)
62.614	1.7222	(102)	(10-12)
75.158	1.4673	(110)	(11-20)
84.595	1.3297	(103)	(10-13)
92.109	1.2428	(112)	(11-22)
93.778	1.2257	(201)	(20-21)

4.2 Hot Rolling

The hot rolling of the sample was performed at 750° C and the sample thickness was reduced from 7 mm to 2 mm over 6 passes. The initial sample dimensions of the plate were 50 mm × 50 mm × 7 mm and rolled to 180 mm × 55 mm × 2 mm. The inter-pass temperature was kept same as the rolling temperature and during each pass ~15-25% deformation was given.

Table 5: Experimental readings from Hot Rolling

Reduction	Roll Load	% Deformation	Strain per Pass
7 mm ➡ 6 mm	618 kgf	14.28	0.1541
6 mm ➡ 5 mm	506 kgf	16.66	0.1823
5 mm ➡ 4 mm	770 kgf	20	0.2231
4 mm ➡ 3.2 mm	707 kgf	20	0.2231
3.2 mm ➡ 2.6 mm	760 kgf	18.75	0.2076
2.6 mm ➡ 2 mm	786 kgf	23.07	0.2623

The hot rolled sample was given a post-deformation heat treatment at 850° C for 1 hour. The post deformation heat treatment was done for generation of a homogenous globularized microstructure. The sample, post deformation heat treatment was cut into pieces and subjected to heat treatment for generation of martensite.

Fig. 28: Initial sample after hot rolling

The final sample is cut into small pieces (of dimensions 10 mm × 10 mm × 20 mm) for heat treatment at different temperature below the beta transus temperature in order to generate different volume fraction of martensite in the Ti-6Al-4V sample. Also, samples for tensile tests and synchrotron study were designed from this hot rolled specimen.

4.3 Heat treatment Schedule

The elongated grains needs to be transformed to equiaxed microstructure in order to have better mechanical properties as compared to hot rolled specimen. The elongated grains could be transformed to equiaxed grains by means of re-crystallization or globularization. The re-crystallization would ensure formation of new strain free grains whereas in case of globularization, equiaxed α morphology is created from elongated grains. As both re-crystallization and globularization are thermally activated processes, it is the surface tension within the α platelets and grain boundaries which causes the globularization to occur. The reasons apart from pinch off from the new grains include substructure formation and dynamic re-crystallization. Therefore, in order to achieve globularization, the deformed samples were annealed at 850°C for 1 hour. The sample is labelled as PDHT-850. The sample is heat treated for martensitic transformation. In order to form martensite for any alloy, the primary condition is to allow cooling at a rate greater than the critical cooling rate. And that the transformation should be from a temperature higher than the Martensitic start temperature (Ms). The Martensitic start temperature for Ti-6Al-4V is around 880°C as per literature.

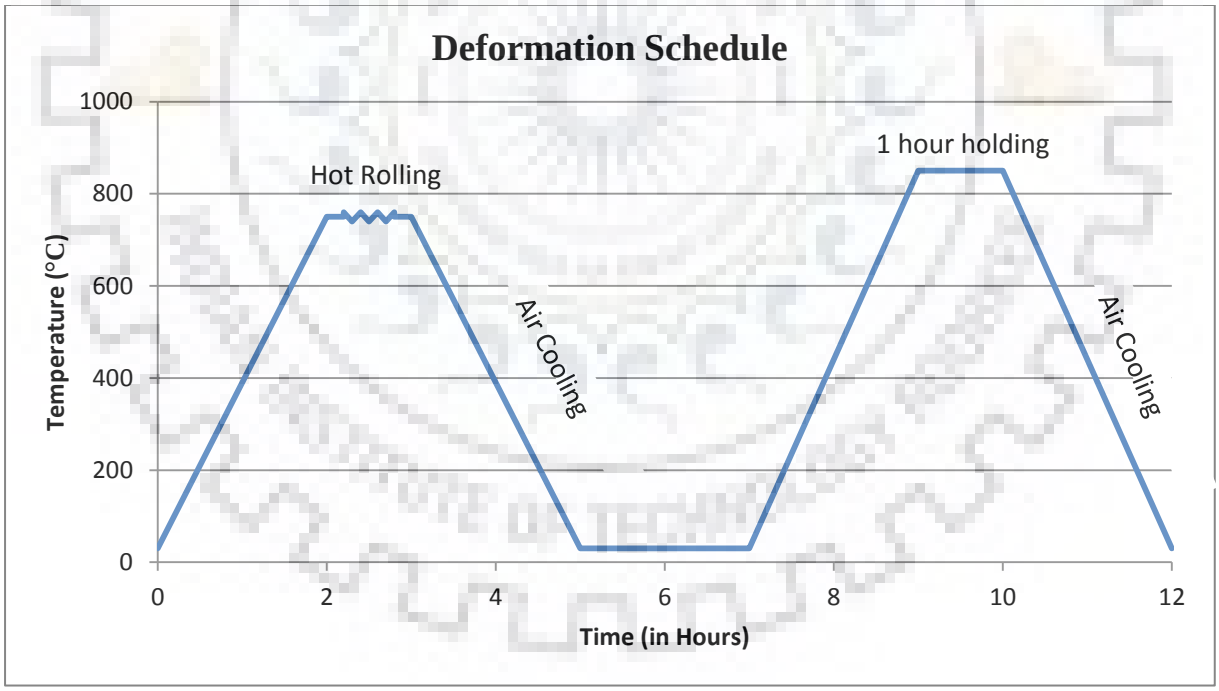

Fig. 29: Deformation Schedule of As-Received Ti-6Al-4V

As the Martensitic start temperature for sample is unknown, the samples are heat treated at temperatures starting from 870°C to 900°C in intervals of 10°C. All the samples were taken to these temperatures of 870°C, 880°C, 890°C, 900°C for 30 minutes and then water quenched. The samples were labelled as WQ870, WQ880, WQ890, WQ900. Also,

samples at a higher temperature of 980°C were water quenched (WQ980) and 950°C air cooled (AC950) in order to observe the microstructural evolution at a considerable higher temperature (As per Fig. 30).

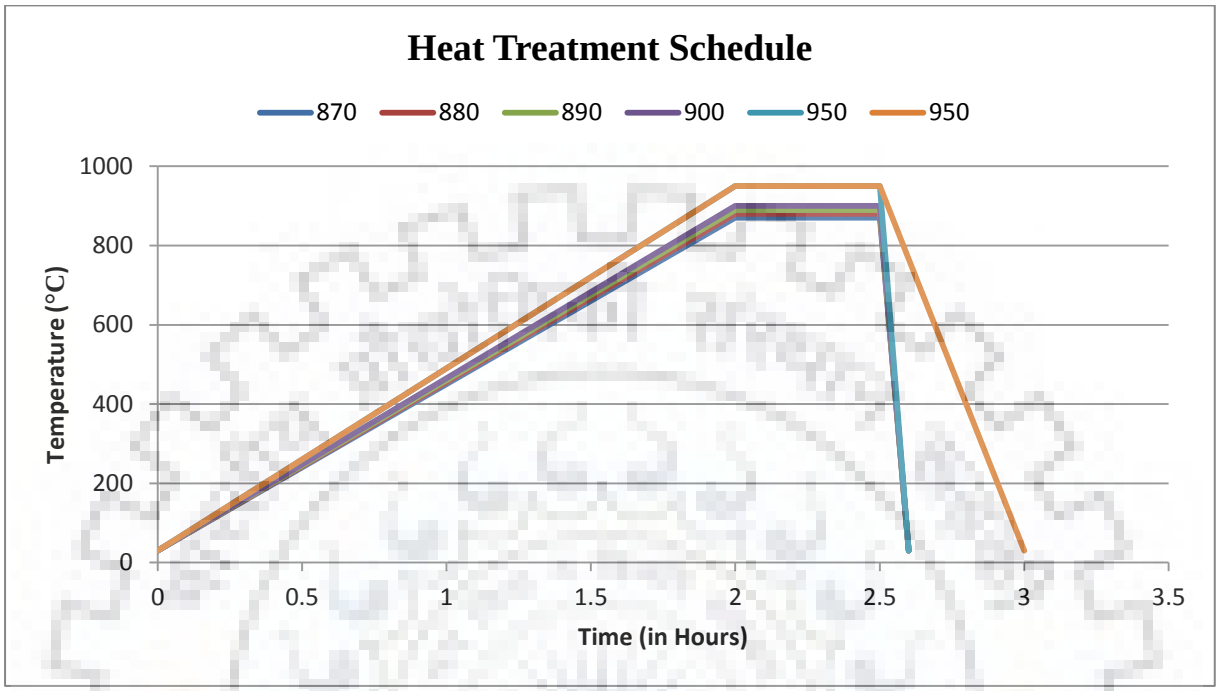

Fig. 30: Heat Treatment Schedule

4.4 Tensile and Synchrotron Study

The deformed samples after generation of martensite were designed with respect to DIN Standards for tensile tests as well as synchrotron study. The specimens followed the Code DIN 50125 (2004) as shown in Fig. 31.

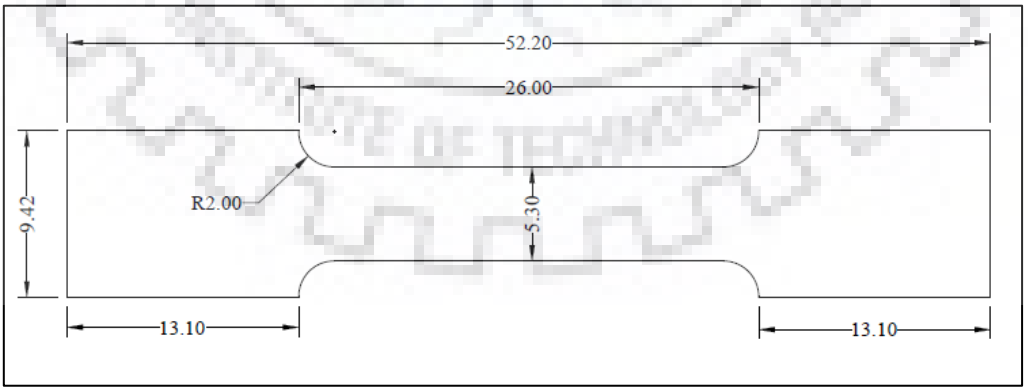

Fig. 31: Design of tensile specimen as per DIN 50125 (All dimensions in mm)

5.0 RESULTS AND DISCUSSION

5.1 Generation of Equiaxed Microstructure

The hot rolled sample has a banded microstructure consisting of elongated grains of α, with β phase at the grain boundaries. The microstructure of hot rolled sample are given in Fig. 32.

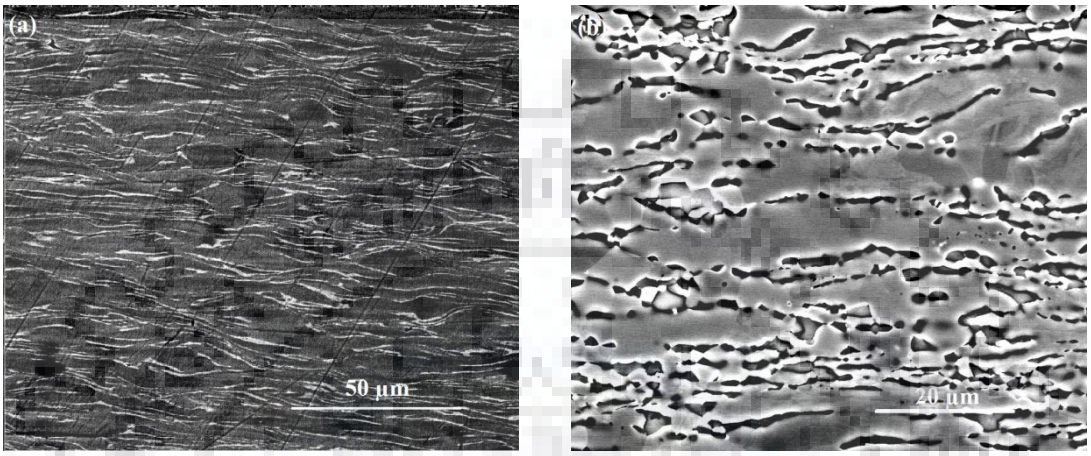

Fig. 32: Sample after hot rolling at 750°C at magnification (a) 1000X (b) 2000X

The chemical composition of different phases present in the hot rolled sample were determined from the SEM-EDS analysis. It was found that the α grain was rich in the aluminium content, whereas at the grain boundary, vanadium enrichment was observed indicating the β phase.

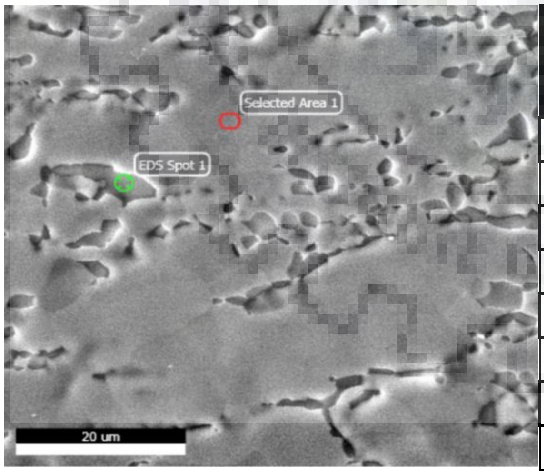

Region of Interest	Element	Weight %	Atomic Wt%
Selected Area 1	Ti	89.37	85.13
	Al	6.72	11.37
	V	3.9	3.49
EDS Spot 1	Ti	84.72	82.64
	Al	4.1	7.11
	V	11.18	10.25

Fig. 33: Energy Dispersive Spectroscopy of α and β phases in Hot-Rolled Ti-6Al-4V

The hot rolled sample PDHT-850 transformed to a recrystallized equiaxed microstructure consisting of globular α, as shown in Fig 34..During the post deformation heat treatment, there was relieving of the stresses and the re-arrangement of the elongated grains

in order to form homogenous, globular α. This was achieved as the temperature for re-crystallization was set above 800°C in order to have enough time for re-crystallization.

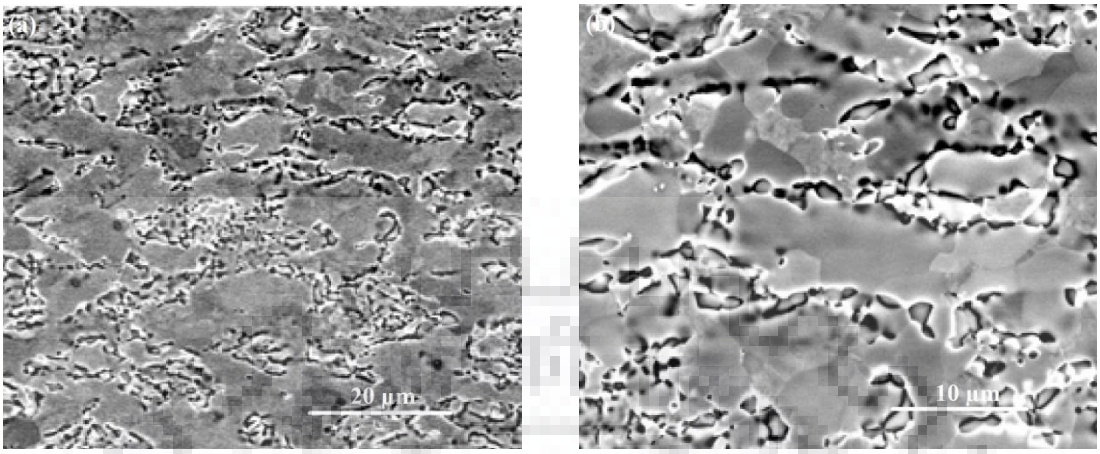

Fig. 34: Post Deformed Heat Treated annealed at 850°C (PDHT-850)

Sample at (a) 2000X (b) 4000X

The intensities for β peaks in XRD were too low due to low volume fraction of the β phase. The first peak for β of $(110)_\beta$ was observed between the peaks of $(0002)_\alpha$ and $(10\text{-}11)_\alpha$, although no other peaks for the β phase was observed in the hot rolled and annealed sample. The first three peaks obtained for α were found at the 2θ values of 41.36°, 45.079°, 47.316° for the planes of (10-10), (0002), (10-11) respectively. The first and only β peak observed was of low intensity at 45.975°. The peaks at higher values of 2θ had (10-12) and (11-20) at 62.77° and 75.42° respectively. The corresponding plots for XRD of as received and AC850 are given as in Fig. 35.

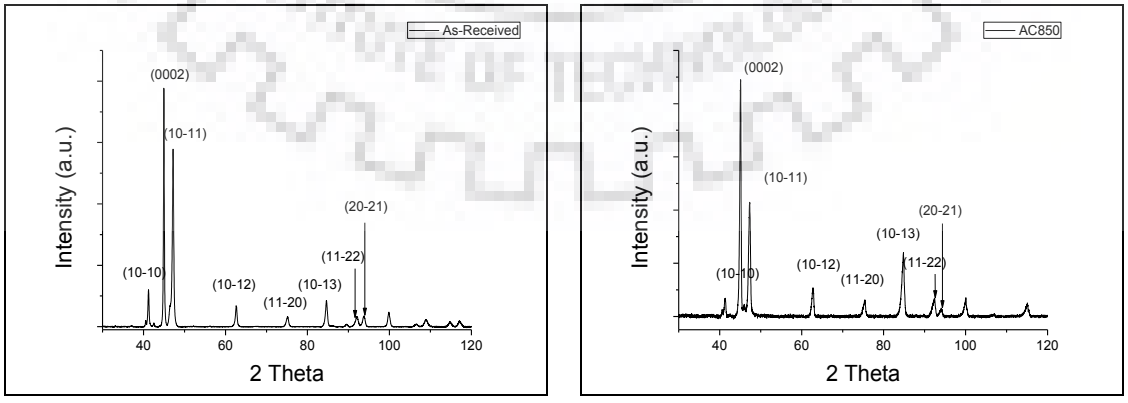

Fig. 35: X Ray Diffration of samples of condition (a) As-Received (b) PDHT-850

5.2 Formation of Martensite

The microstructures of the WQ870 given in Fig. 36 show the presence of only equiaxed grains. The equiaxed grains are the resultant of globularization combined with recrystallization, during post heat treatment.

Fig. 36: BSE SEM Image of WQ870 Sample

The sample at WQ870 had nearly no lamellar morphology and it was also expected that the grains would only coarse. Thus, the structure is ~100% equiaxed with an average grain size of 1.5 µm as observed in the SEM. The phase fraction consists of globular α with the β phase present only at the grain boundaries. The sample is similar to heat treated sample post rolling, just that the grains have re-arranged to form more globular and coarse structure. The microstructure of WQ880 shows a majority of equiaxed grains but a few of the grains have lamellar morphologies, a part of these lamellar features could be martensite (Fig. 37). The fraction of these lamellar morphologies is very small.

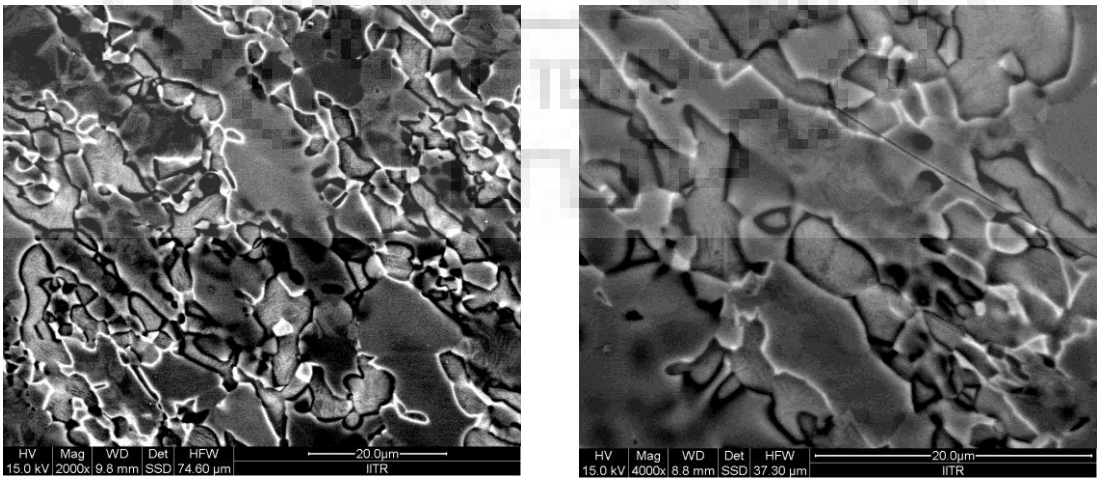

Fig. 37: BSE SEM Image of WQ880 Sample

The sample at WQ880 has started to generate lamellae at certain places. Since the temperature is around the M_s temperature, it could be possible that the temperature has gone above the M_s temperature and the cooling rate is evident enough to initiate the formation of martensites. The nucleation of the martensites starts from the diffusionless transformation of the β phase that transform itself into α′ martensite.

Table 6: WQ870 Morphology Distribution

Morphology of 870°C	Avg. Area (μm^2)	Number of Grains	Total Area (μm^2)	(Morphology Fraction %)
Equiaxed	127	41	5207	~100 %
Lamellar	0	0	0	~0 %

Table 7: WQ880 Morphology Distribution

Morphology of 880°C	Avg. Area (μm^2)	Number of Grains	Total Area	(Morphology Fraction %)
Equiaxed	145	34	4930	94.69%
Lamellar	69	4	276	5.30%

The EBSD pattern for the WQ870 and WQ880 give more insight regarding the morphology present within them. The IPF Map and IQ Map for the WQ870 and WQ880 samples are shown as in Fig. 38 and Fig. 39. The EBSD scan that was taken for both the samples was done at step size of 0.3 μm and the pattern was found to have a confidence index of 0.8.

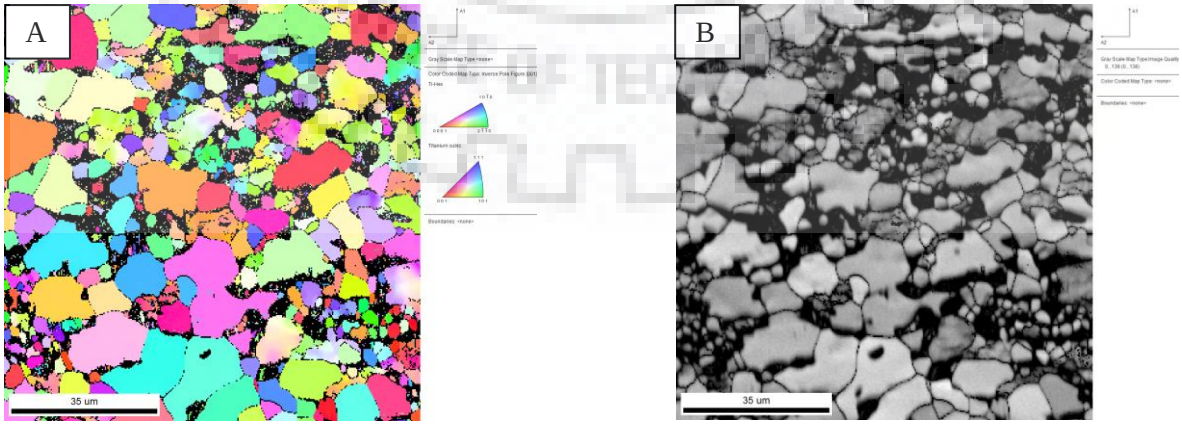

Fig. 38: EBSD scan of WQ870 Sample (a) IPF Map (b) IQ Map

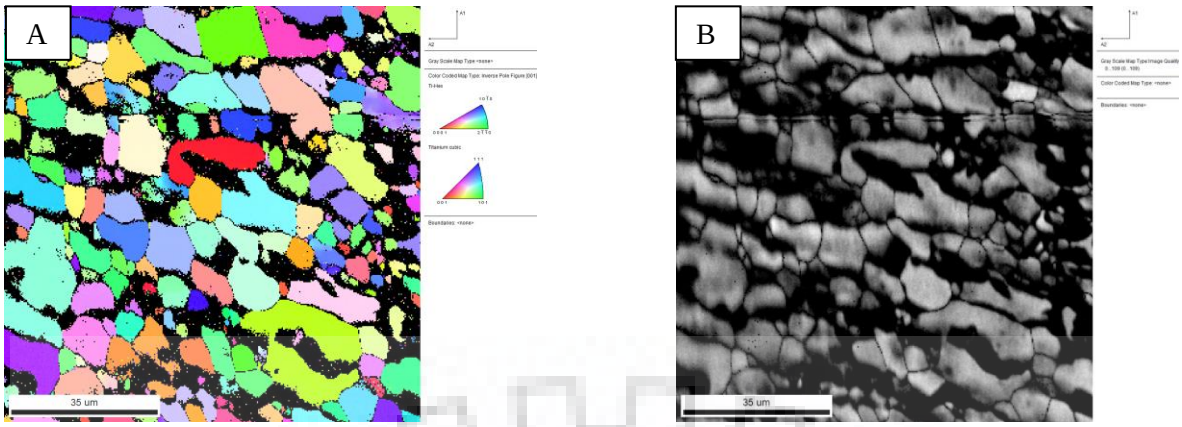

Fig. 39: EBSD scan of WQ880 Sample (a) IPF Map (b) IQ Map

The grain size distributions for the samples are represented by plots of number and area fraction vs grain size (diameter) (Fig. 40 and 41). For WQ870 sample, the average size of grain is 5.3 µm and for WQ880 sample it is 7.6 µm. The average area for grain size of WQ870 sample is 9.65 μm^2 and WQ880 sample is 10.28 μm^2. The increase in grain size (diameter and area) may be due to coarsening at higher temperature.

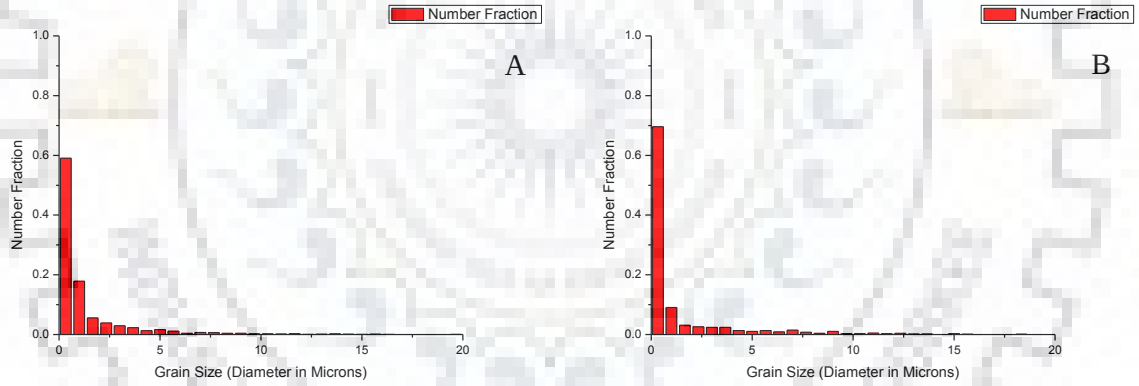

Fig. 40: Grain Size Diameter (Number Fraction) of WQ870 and WQ880 Samples

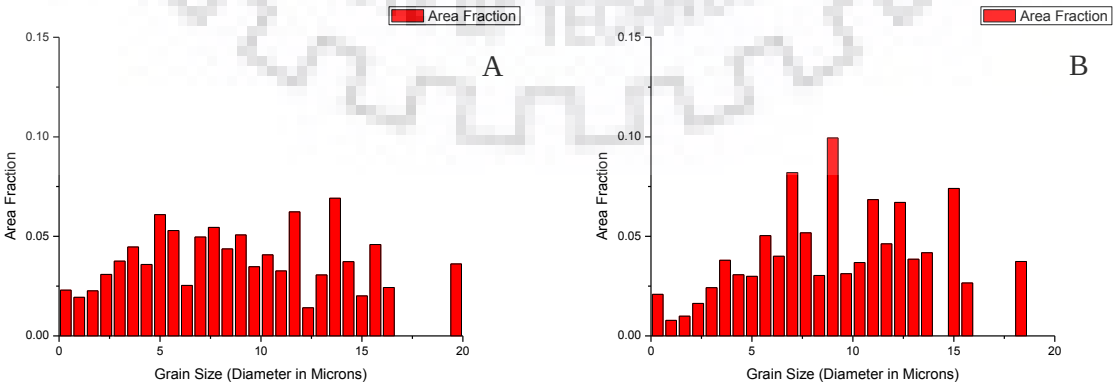

Fig. 41: Grain Size Diameter (Area Fraction) of WQ870 and WQ880 Samples

The aspect ratio for samples were calculated and plotted in Fig. 42 and Fig. 43. The average aspect ratio for the grain size distribution for WQ870 was 0.54. and for the WQ880 sample was 0.50. The decrease in aspect ratio indicates formation of lamellae structures at places. There is increase in area fraction for aspect ratio below 0.4 indicating lamellae morphology starts to occur.

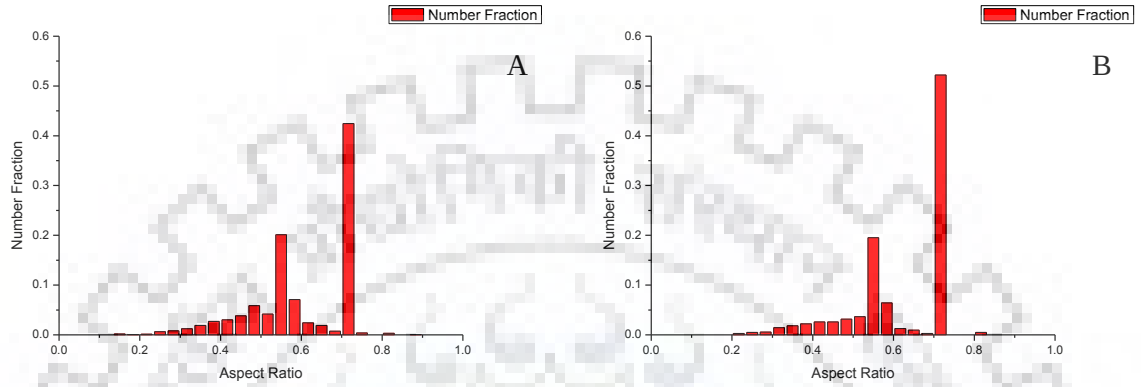

Fig. 42: Aspect Ratio (Number Fraction) of WQ870 and WQ880 Samples

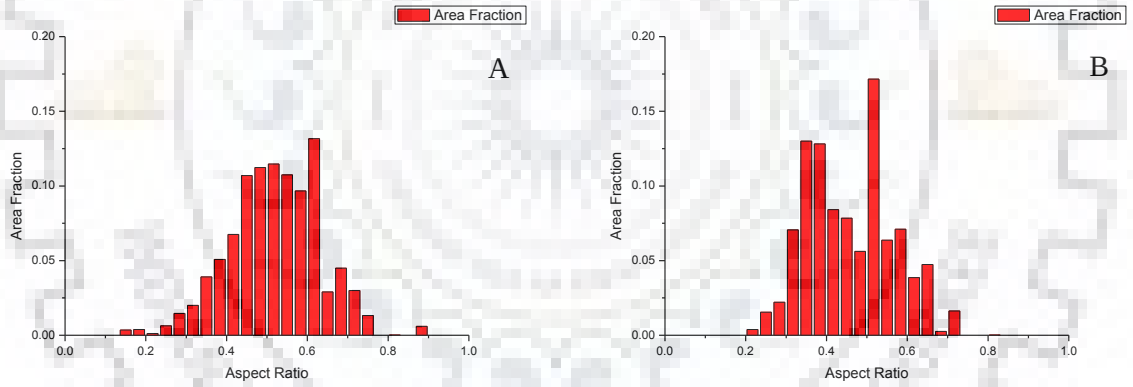

Fig. 43: Aspect Ratio (Area Fraction) of WQ870 and WQ880 Samples

The misorientation angle distribution for WQ870 and WQ880 samples are provided in Fig. 44. The fraction of grains with lower misorientations (<40%) are higher for WQ870 sample when compared with the WQ880 sample. No major difference is observed between correlated and uncorrelated misorientation distributions. Here, correlated misorientation represent misorientations with only first nearest neighbour, where as uncorrelated misorientation calculates misorientations of a single grain with respect to all other grains in the scan. Also, the number fraction of misorientations for both the sample lay below 10% indicating the misorientations could be varying and not specific to a particular value.

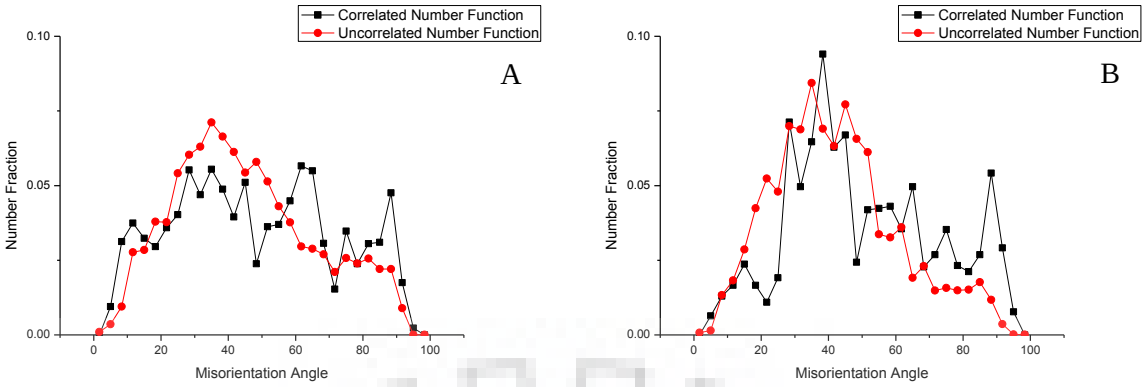

Fig. 44: Misorientation Angle for (a) WQ870 (b) WQ880 Samples

The WQ890 and WQ900 samples consists of both equiaxed as well as lamellar morphologies (Fig. 45 and Fig. 46). Lamellar structures have evolved during the post heat treatment and quenching has resulted in the formation of fine martensite phases within the lamellar regions, while presence of martensite within the equiaxed morphology is not visible. This could be explained on the fact that the martensite phase forms from the high temperature bcc structure while not from the hcp phase. All the grains that have transformed to the high temperature bcc structure will transform as lamellar morphology, while the equiaxed grains that remain as un-transformed structure cannot undergo the martensitic transformation.

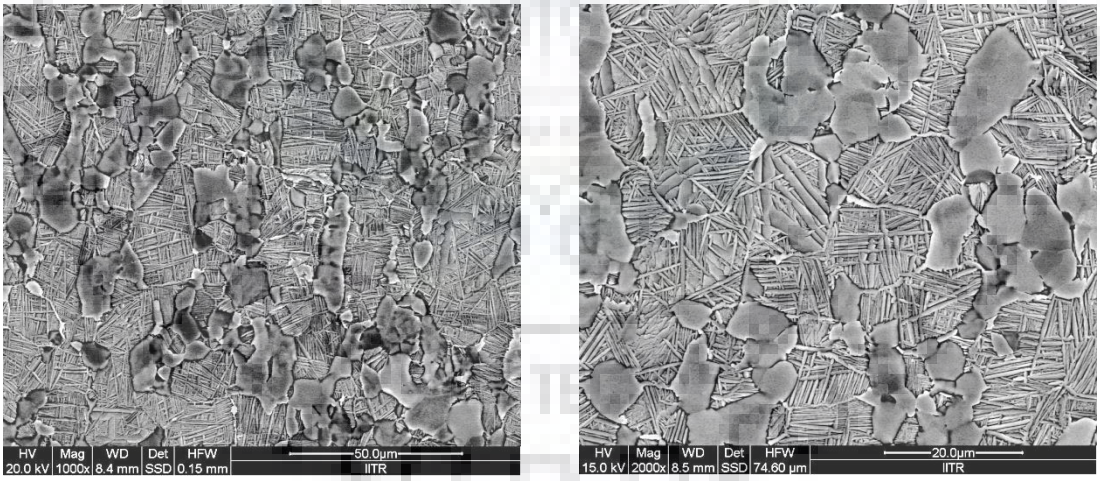

Fig. 45: BSE SEM Images for the WQ890 Sample

The fraction of equiaxed morphology is lower for WQ900 sample and the corresponding fractions of different morphologies of WQ890 and WQ900 are provided in Table 8 and 9 respectively.

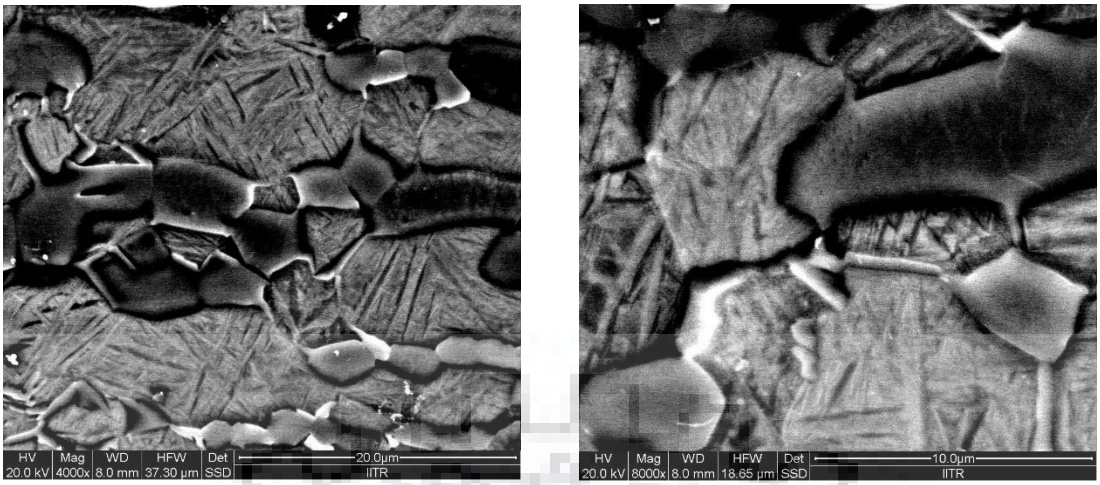

Fig. 46: BSE SEM Images for the WQ900 Sample

Table 8: WQ890 Morphology Distribution

Morphology of 870°C	Avg. Area (μm^2)	Number of Grains	Total Area (μm^2)	(Morphology Fraction %)
Equiaxed	62	28	1736	33.18%
Lamellar	92	38	3496	66.81%

Table 9: WQ900 Morphology Distribution

Morphology of 870°C	Avg. Area (μm^2)	Number of Grains	Total Area (μm^2)	(Morphology Fraction %)
Equiaxed	97	14	1358	26.25%
Lamellar	212	18	3816	73.75%

Also, a higher temperature (close to β transus, 980°C) was chosen to observe the microstructure obtained by quenching. It was found that there is complete transformation of the equiaxed morphology into fine lamellar structures, which turn to be martensites (Fig. 47).

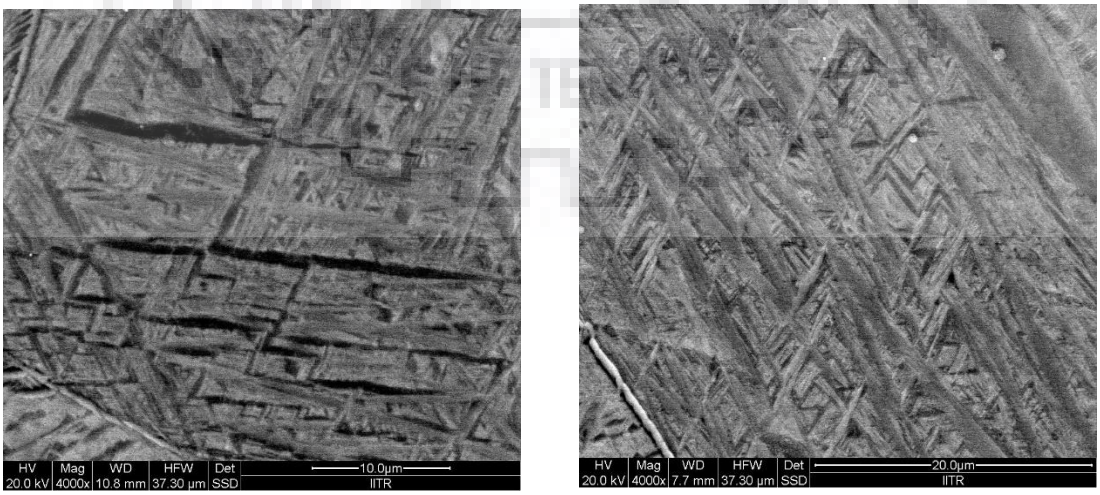

Fig. 47: BSE SEM Images for the WQ980 Sample

The transformation at 980°C display completely transformed structure with significant amount fraction of acicular martensite (Table 10). No globular structure is found, suggesting the material has gone above the beta transus temperature. The transformation has taken place from β to α′ because of high temperature and rapid cooling. These acicular martensites have grown along all regions, in an inter-penetrating fashion with primary as well as secondary and tertiary needle like structures. Thus, going for temperatures above 980°C won't be beneficial. The temperature range 880°C-900°C is useful for the generating martensite.

Table 10: WQ980 Morphology Distribution

Morphology of 870°C	Avg. Area (μm^2)	Number of Grains	Total Area (μm^2)	(Morphology Fraction %)
Equiaxed	N.A.	N.A.	0	~0
Lamellar	N.A.	N.A.	5212	~100%

The different morphology fractions against quenching temperature condition for all 5 water quenched conditions are shown in Fig. 48.

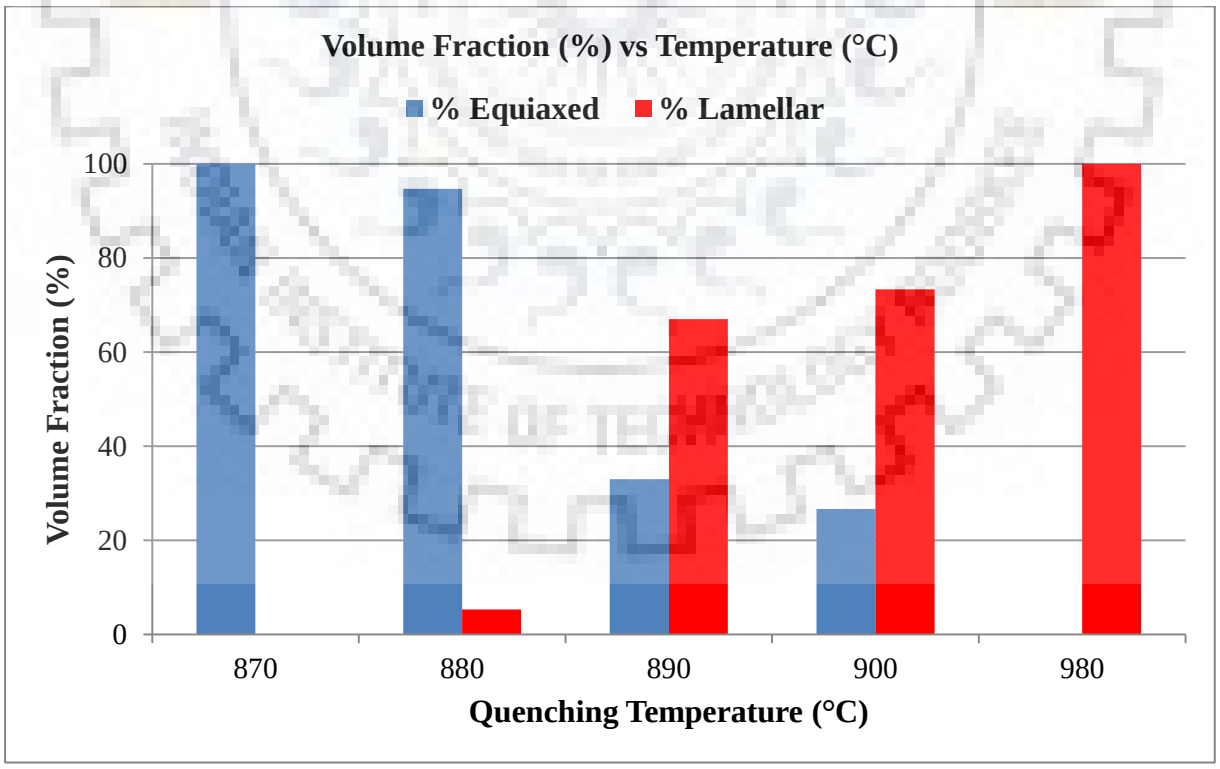

Fig. 48: Plot for morphology distribution

Alternative to quenching, air cooling for the deformed sample at 950°C was done. This was in order to ensure that the cooling rate is steady, as compared to that of quenching. It also allowed less of acicular martensites and retention of regions of equiaxed α. The following microstructures as in Fig. 49 depict the equiaxed as well as lamellar morphology when air cooled from 950°C.

Fig. 49: AC950 Morphology Distribution

Table 11: AC950 Morphology Distribution

Morphology of 870°C	Avg. Area (μm^2)	Number of Grains	Total Area (μm^2)	(Morphology Fraction %)
Equiaxed	94	17	1598	30.81%
Lamellar	138	26	3588	69.18%

The distribution of morphology plays an important role in the mechanical properties of any material. The equiaxed microstructure tends to possess more ductility whereas the lamellar structures are useful in building the strength of the material. In order to get the perfect combination of strength as well as ductility, there is a need to optimize the composition of Ti-6Al-4V such that there are as much equiaxed regions as lamellar structures. Considering this need to obtain good mechanical properties, it is important to understand the role of martensite in the sample, hence, the EBSD scans for 890°C and 950°C samples were done.

The IPF and IQ Map for the WQ890 and AC950 samples are generated using the TSL OIM Software. The scan rate was kept 0.2 µm and confidence index for both the samples was above 0.2. The Fig. 50 and Fig. 51 gives a comparative study of both the IPF and IQ Map.

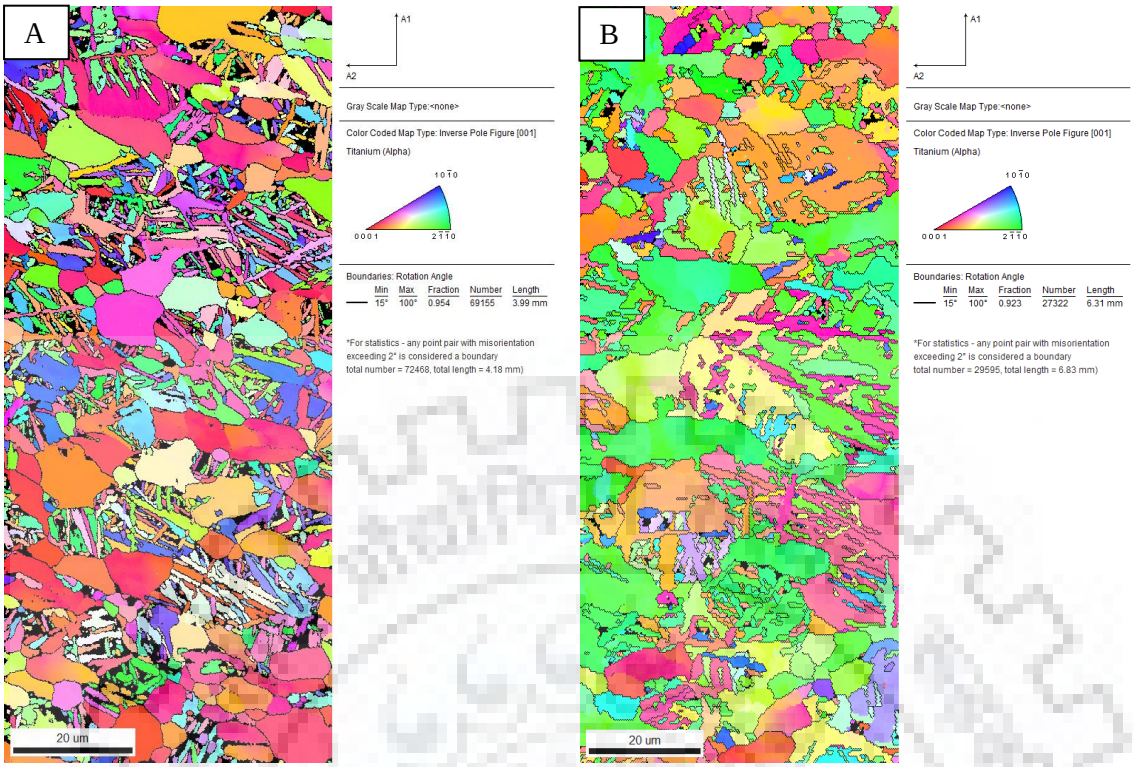

Fig. 50: IPF Maps for (a) WQ890 Sample, (b) AC950 Sample

The IQ Map for the scans are as follows :

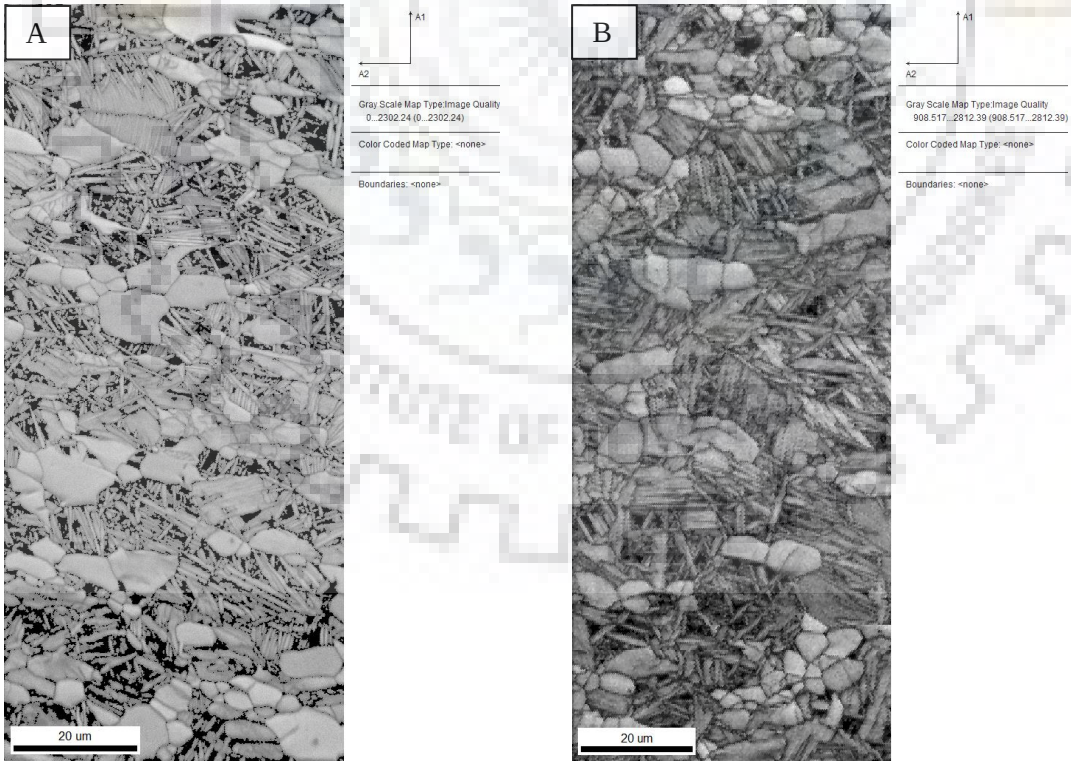

Fig. 51: IQ Maps for (a) WQ890 Sample, (b) AC950 Sample

WQ890: Initially, let us consider one of the regions of the WQ890 sample and obtain a misorientation profile scan, for both the lamellar as well as the equiaxed regions. The misorientation profile along A and B in the below picture denotes the distance vs misorientation profile for equiaxed (Fig. 52A) as well as lamellae (Fig. 52B) fractions. It has been observed that the misorientation angle for equiaxed is lower than 2°, whereas in case of lamellar it is much much higher. Hence, the definition for equiaxed and lamellar would now be for misorientation within a grain if greater than 2°, would be lamellar, else, equiaxed. The values for lamellar also follow a particular misorientation angle value, rather than any random arbitrary value, hence showing the preference of one orientation over another.

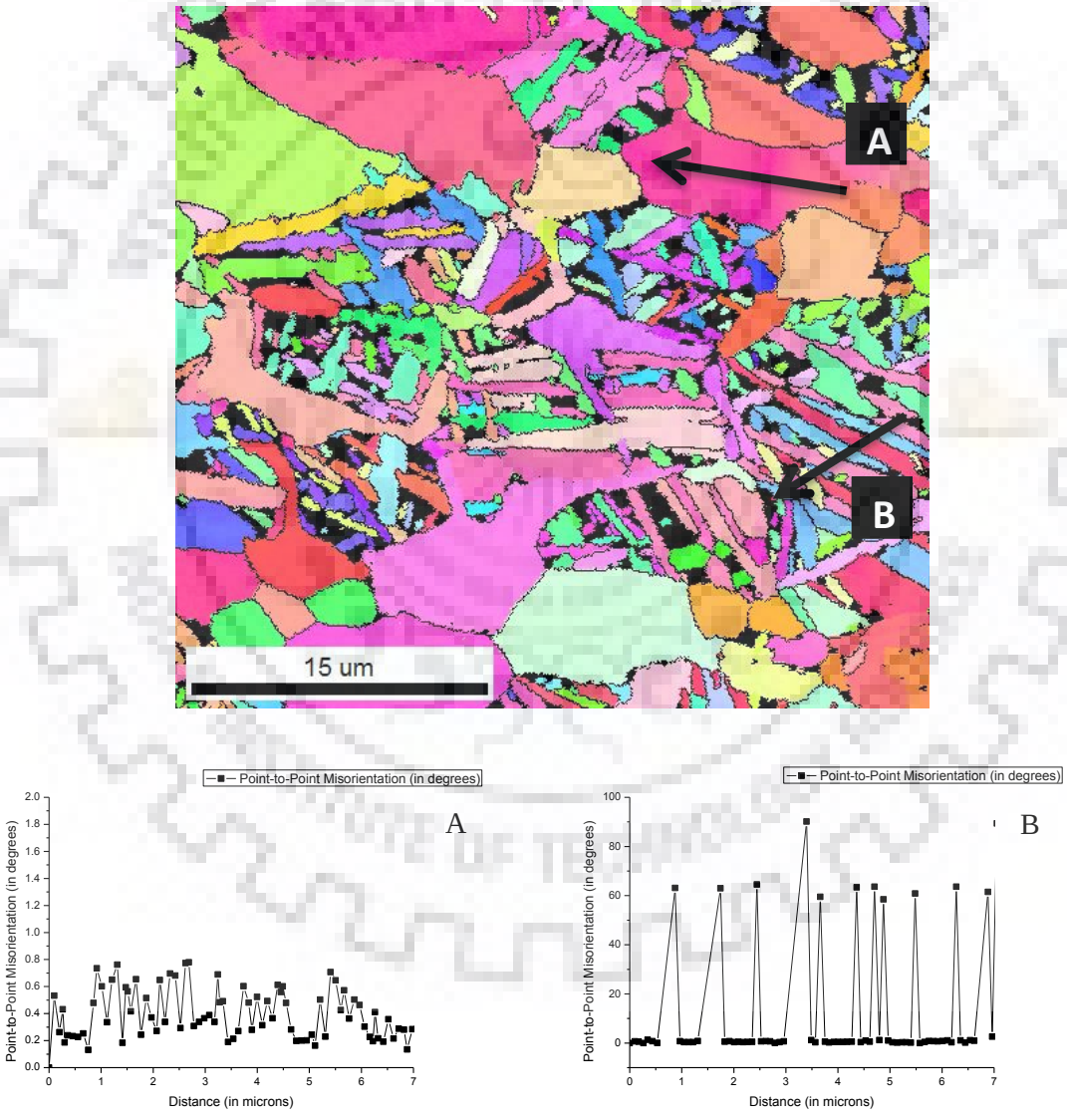

Fig. 52: A section of WQ890 showing equiaxed (A) as well as lamellar (B) region in IPF Map. Misorientation profile (Point-to-Point Misorientations) along A and B were taken. (a) Misorientations along A (b) Misorientations along B.

950 AC: The EBSD for AC950 have been split into lamellar as well as equiaxed region on the basis of misorientation angle within a grain. The IPF and IQ Map is as below (Fig. 53 A and Fig. 54 A for Equiaxed Region and Fig. 53 B and Fig. 54 Bfor Lamellae Region).

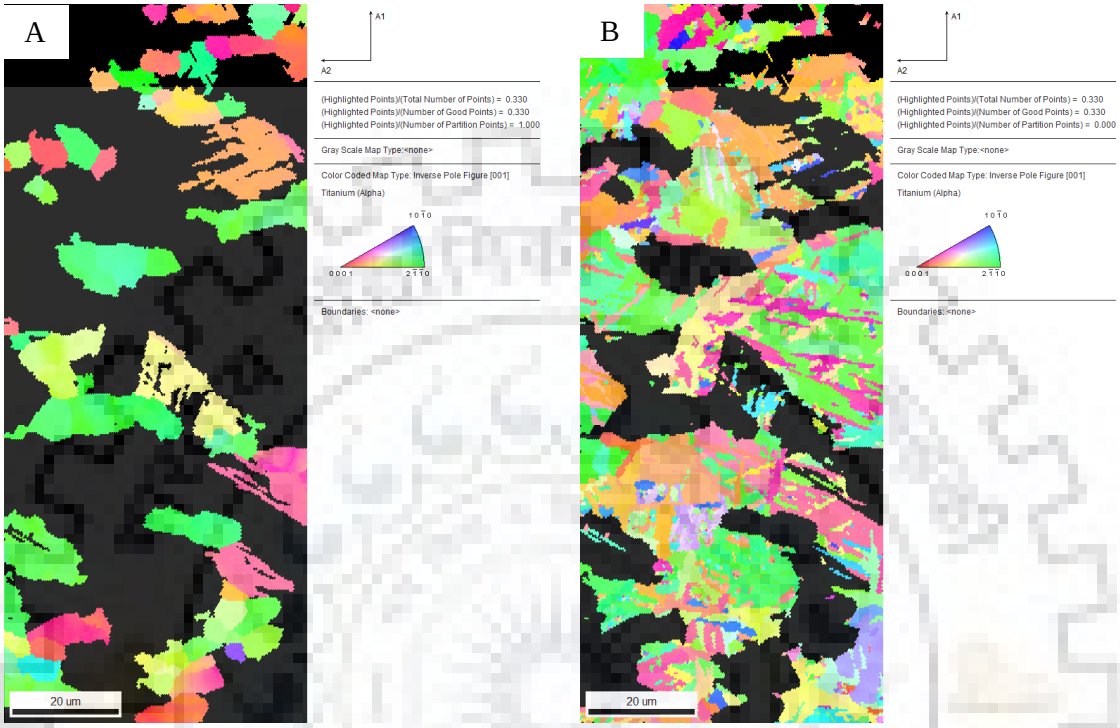

Fig. 53: IPF Map for AC950 Sample containing (a) Equiaxed (b) Lamellar region

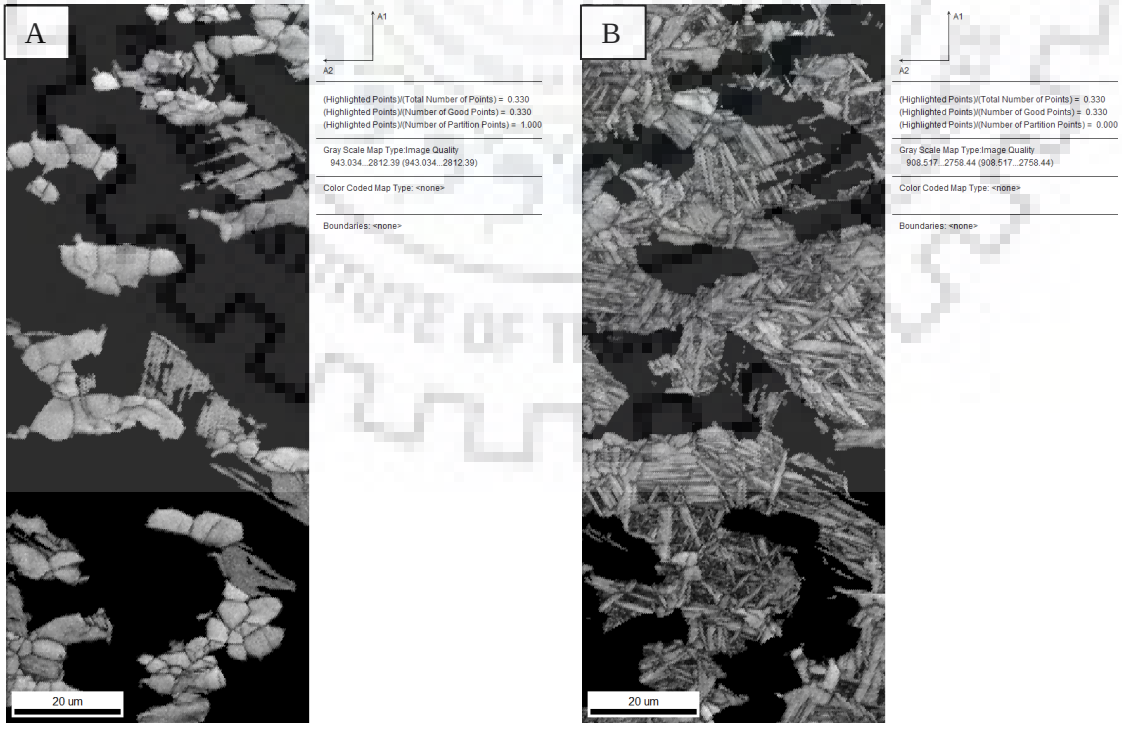

Fig. 54: IQ Map for AC950 Sample containing (a) Equiaxed (b) Lamellar region

The misorientation angle distribution for the region of equiaxed and lamellar were plot separately, in order to understand the difference. The equiaxed regions showed a number fraction of less than 10% for all the misorientation angles from 0° to 100°, indicating a good probability for any of the misorientation to take place within an equiaxed grain. There was a drastic difference in the number fraction for the lamellar regions. In case of correlated number fraction, there existed three different peaks at 10°, between 60° and 63° and at 90°. The significance of these three misorientations to take place in all probable regions could be due to the formation of martensite.

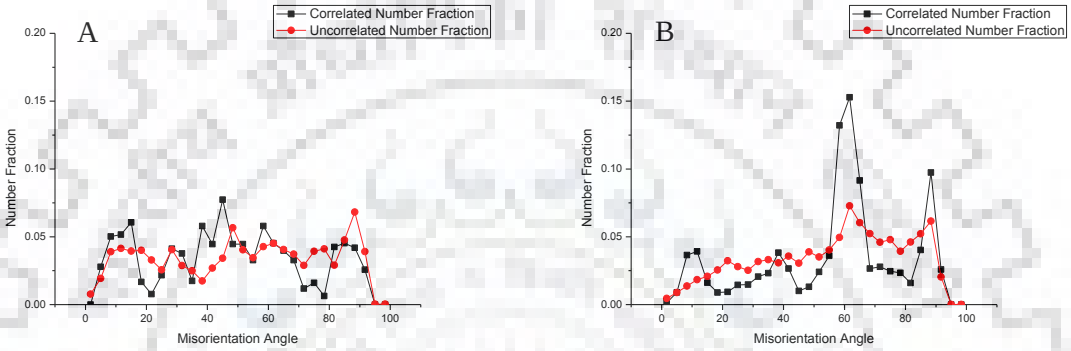

Fig. 55: Misorientation Angle (Number Fraction) for (a) Equiaxed (b) Lamellar Region

The Axis/Angle Distribution in case of Equiaxed and Lamellar shows the misorientation of grains with respect to the sample orientations. It is observed that in case of equiaxed the majority of the points lie in the 0° whereas for lamellar they are concentrated in 10°, 60° and 90°. The Axis/Angle Distribution concentration accounts for the planes in which they are concentrated which shows that majority of the planes are contained within the sample.

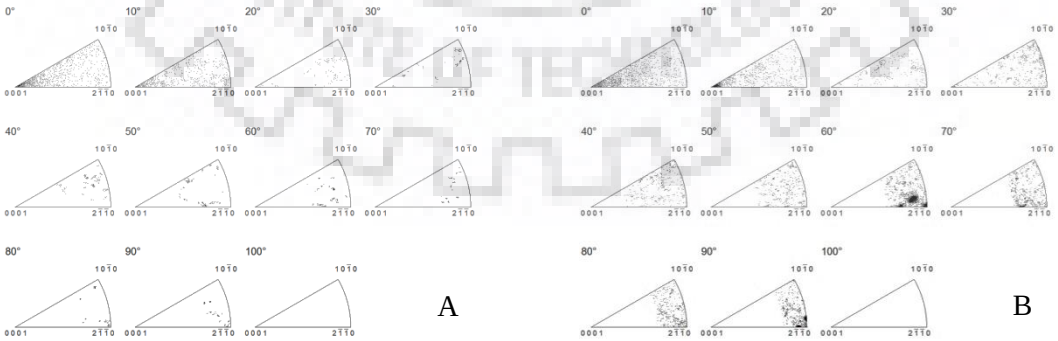

Fig. 56: Axis/Angle Distribution Plots for (a) Equiaxed (b) Lamellar Region

Thus, it can be inferred that certain planes in case of lamellar have the tendency to orient themselves in a particular misorientation when they transform from β phase to transformed α. This transformed α forms along with fine α′ and these planes signify the α′.

The lamellar phase α and the martensite α′ obtained as in the samples of WQ900 and WQ980 were to be characterized for further study. In order to study the role of martensite on the deformed Ti-6Al-4V sample, X ray diffraction of these samples were done. The plots for the Intensity vs 2θ for both the samples are given below.

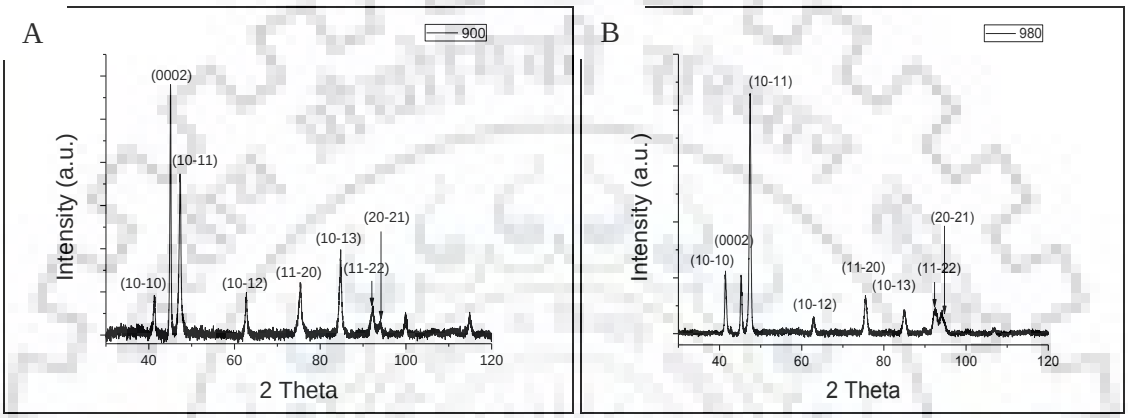

Fig. 57: XRD Analysis of (a) WQ900 (b) WQ980 Samples

The peaks observed in case of deformed samples at 900°C and 980°C were similar to the peaks obtained for the heat treated sample at 850°C. The peaks for martensite were difficult to characterize as the intensity for these peaks were relatively low in comparison and at the same location to that of peaks for α phase. Thus, the conventional X ray diffraction proved to be a limitation to distinguish the peaks for the α and α′ phase. Therefore, in order to characterize for martensite, the newer technique for measuring the x ray diffraction along with deformation can be studied with synchrotron x ray diffraction.

5.3 Effect of Martensite on Deformation

Tensile Test : The mechanical properties are of major concern for any material. In order to look for mechanical properties the samples were tensile tested. The tensile test was done for two samples i.e one without lamellae (WQ880) and one with ~73% volume fraction of lamellar (WQ900). The stress-strain plots obtained from the tensile tests are shown below in the graphs.

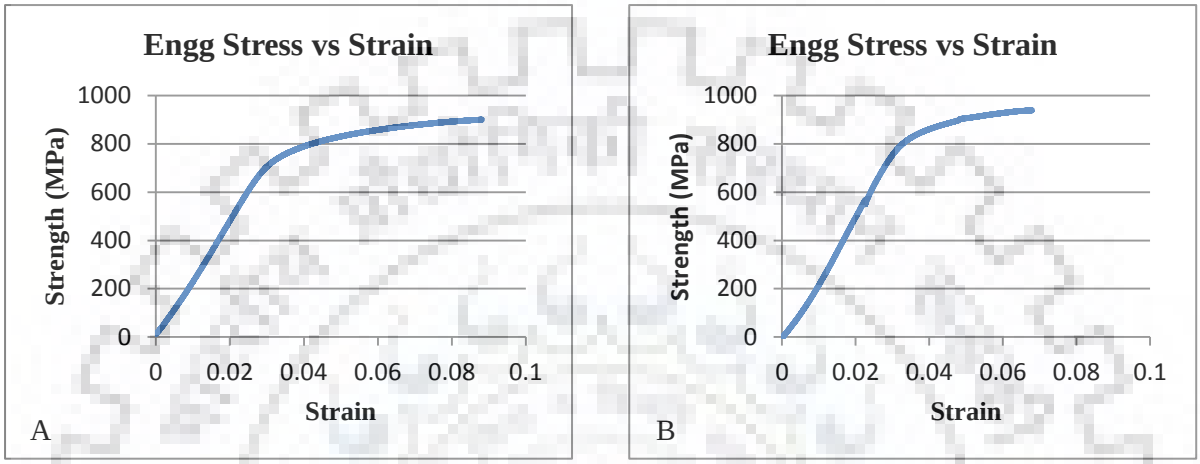

Fig. 58: Stress-Strain Plots for (a) WQ880 (b) WQ900 Samples

The ultimate tensile strength obtained by the 880°C sample was 899 MPa whereas that for the 900°C sample was found to be 938 MPa. The ductility was much higher for the 880°C case as compared to that of 900°C sample due to absence of martensite or presence of equiaxed morphology. The martensite present in the form of needles helps to increase of strength for the 900°C sample but at the cost of ductility. The ductility obtained for 900°C sample is only 7% whereas in case of 880°C, it is much higher at 9%.

The tensile specimen was subjected to fractography analysis. The fractured specimens showed distinct features. The sample with no martensite showed a cup and cone type ductile fracture surface, whereas the sample with martensite showed fibrous type of fracture. The depth of the dimples correlates to the ductility for the sample. It was observed that the sample at WQ880 had more depth in dimples than the WQ900 sample.

Corresponding to the fracture, the near edge region of the fractured specimen was observed in SEM for the deformation induced changes in microstructure, if any, have taken place. The SEM image for the near fracture edge region are as shown in Fig. 59 (a) and (b) . It was observed from these images that the pre-tensile and post-tensile specimen had significant changes in microstructure.

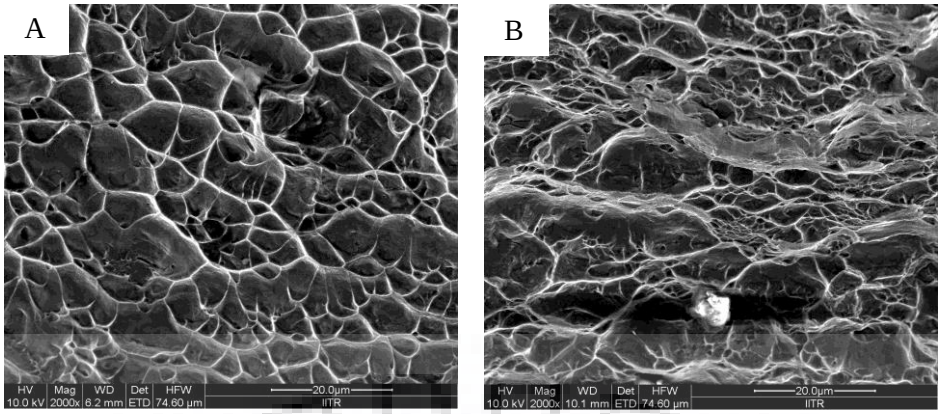

Fig. 59: Fractographs for (a) WQ880 (b) WQ900 Samples

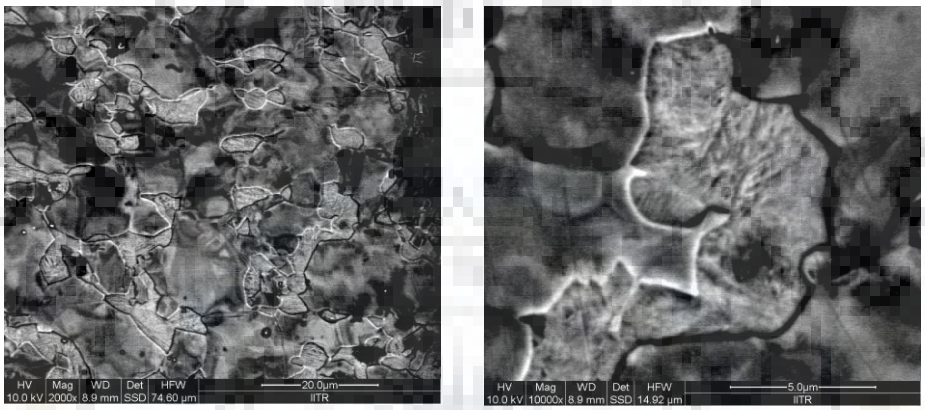

Fig. 60: Microstructure of WQ880 sample near-fracture edge

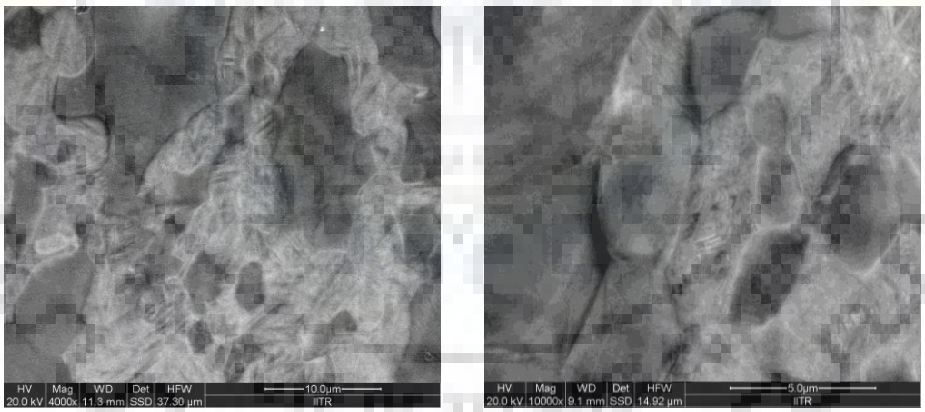

Fig. 61: Microstructure of WQ900 sample near-fracture edge

Synchrotron Study : The study of deformation along with diffraction using synchrotron are present in this section for samples that contain significant fractions of martensite. Thus, two samples of WQ880 and WQ900 were deformed in tension and the corresponding changes in diffraction patterns during deformation were characterized. The values for d spacing with respect to stress at different azimuthal angles of 0°, 45° and 90° were found out by fitting the plot of Intensity vs 2θ using the Single Peak Fit function. These peaks of S-XRD were fit using Pearson VII function. The values for the d spacing vs Stress for various planes with

respect to the WQ880 and WQ900 were observed. Also, the lattice strain for the same was calculated using the following formulae :

$$\text{Lattice Strain} = (d_{final}-d_{initial})/d_{initial} \qquad \text{Macro Strain} = (L_{final}-L_{initial})/L_{initial}$$

Changes in (10-10) Plane: With application of tensile stress along the rolling direction, there is development of compressive strains in the (10-10) plane which are parallel to the loading axis. The compressive strains for (10-10) plane is more for the WQ900 sample than WQ880 sample. For (10-10) planes lying perpendicular to the loading axis, the effect of tensile loading gives a tensile strain which causes increase in d spacings. The planes which lie at 45° to the loading axis show negligible change in the d spacing, hence having neither compressive nor tensile stress. The sample WQ880 exhibits a linear curve whereas for the sample WQ900, the sample exhibits piecewise linear. Presence of martensite in WQ900 could be a possible reason for such changes.

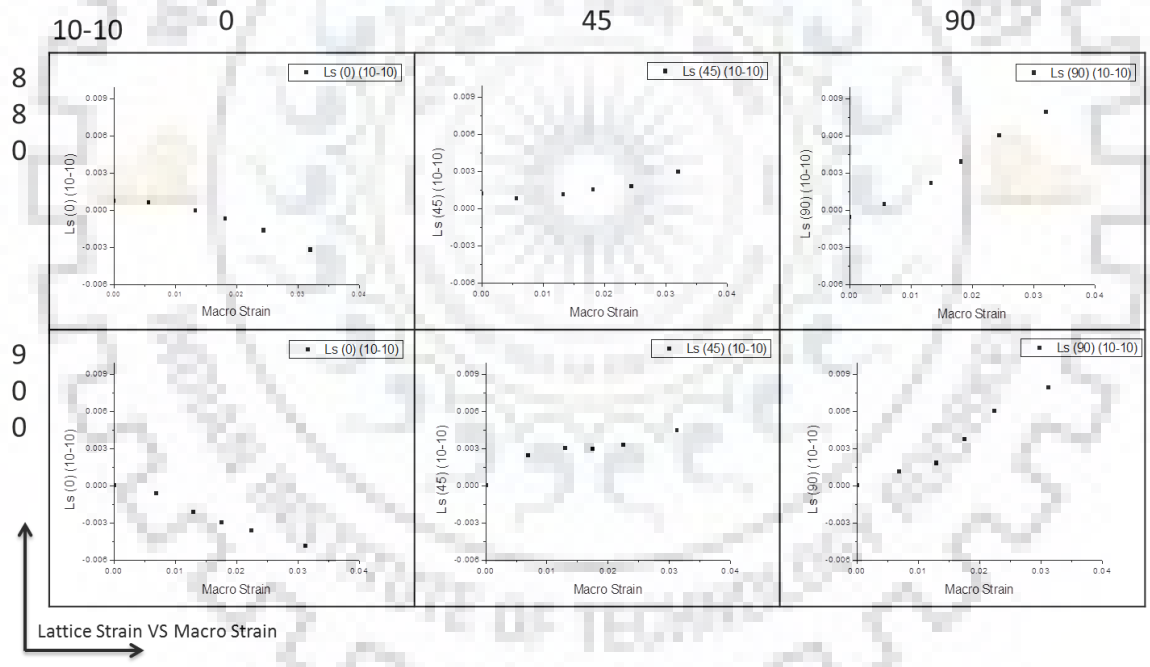

Fig. 62: Lattice Strain vs Macro Strain in (10-10) plane

Changes in (10-11) Plane: (10-11) planes that are parallel to the loading axis exhibit compressive strains while planes perpendicular to the loading axis exhibit tensile strains. For planes, that are lying at 45° to the loading axis, these strains are negligible.

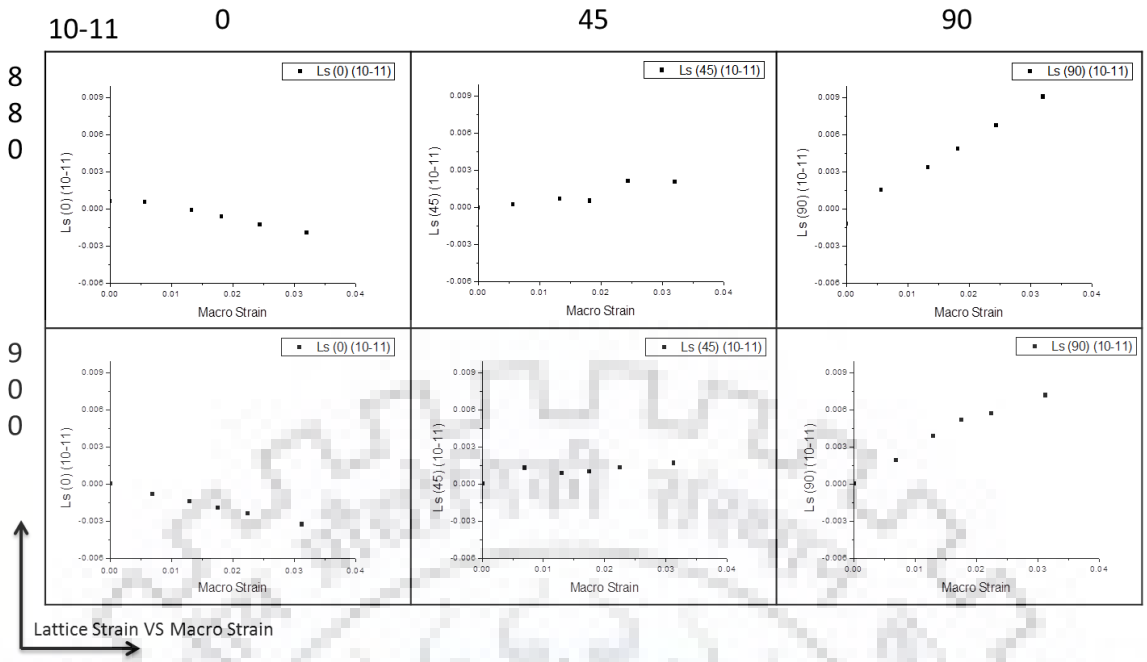

Fig. 63: Lattice Strain vs Macro Strain in (10-11) plane

(10-12) Plane: The compressive stress for WQ880 is much more than for the WQ900 in case of 0° Azimuthal angle. Correspondingly, there is higher tensile stress shown for 90° in case of WQ900 Sample. This could be because of the initiation of deformation at smaller values of elastic stresses leading to more stress concentration near martensite, thereby showing more lattice strain normal to loading axis.

(11-20) Plane: The (11-20) plane exhibits near similar strain values for both the samples. The compressive as well as tensile stresses are developed in good amount owing to the steepness of the slope.

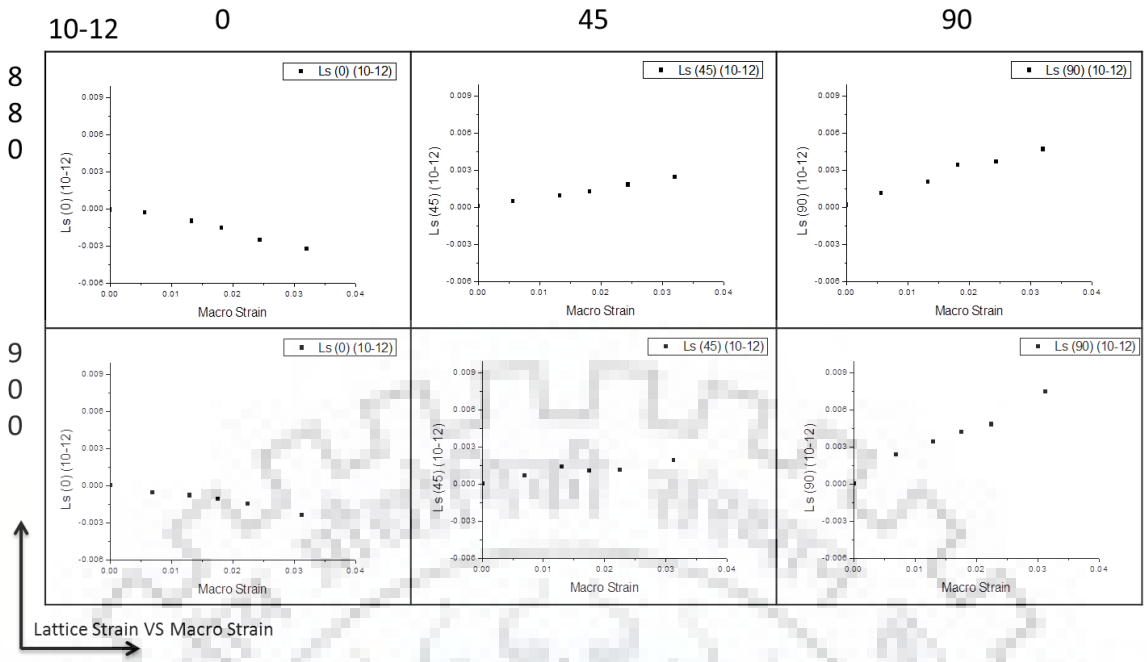

Fig. 64: Lattice Strain vs Macro Strain in (10-12) plane

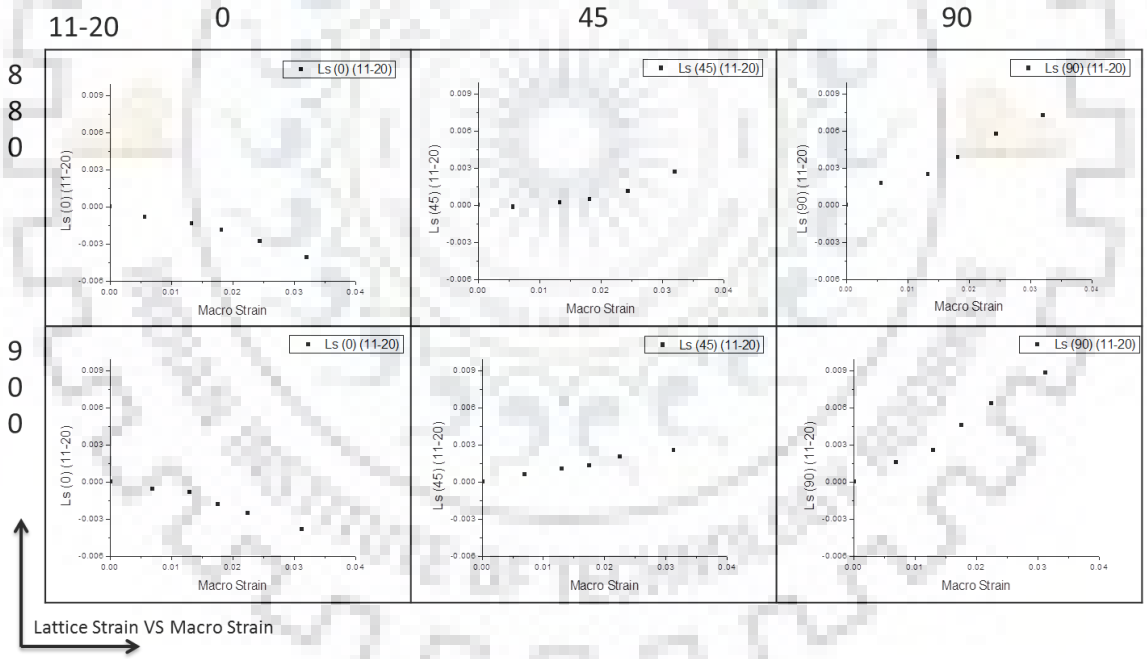

Fig. 65: Lattice Strain vs Macro Strain in (11-20) plane

Texture: The (0002) pole figure displays the distribution of the basal plane (0002) with respect to the sample coordinates. From the Fig. 66 and Fig. 67, it is observed that there exists a strong concentration of (0002) plane lying perpendicular to the RD and a relatively weaker texture presence of (0002) parallel to rolling plane. With deformation, the sample WQ880 and WQ900, there is a negligible change in the texture of both the samples. The sample WQ880 exhibit a stronger overall texture, as compared to the texture for the WQ900 Sample.

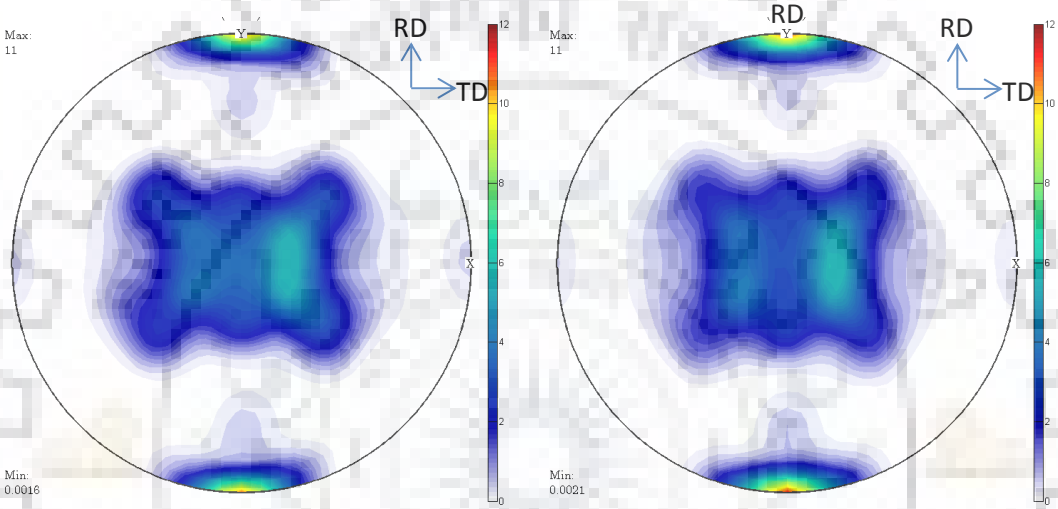

(a) 0.5 mm deformation (b) 1 mm deformation

Fig. 66: Pole Figure for (0002) Plane of WQ 880 Sample

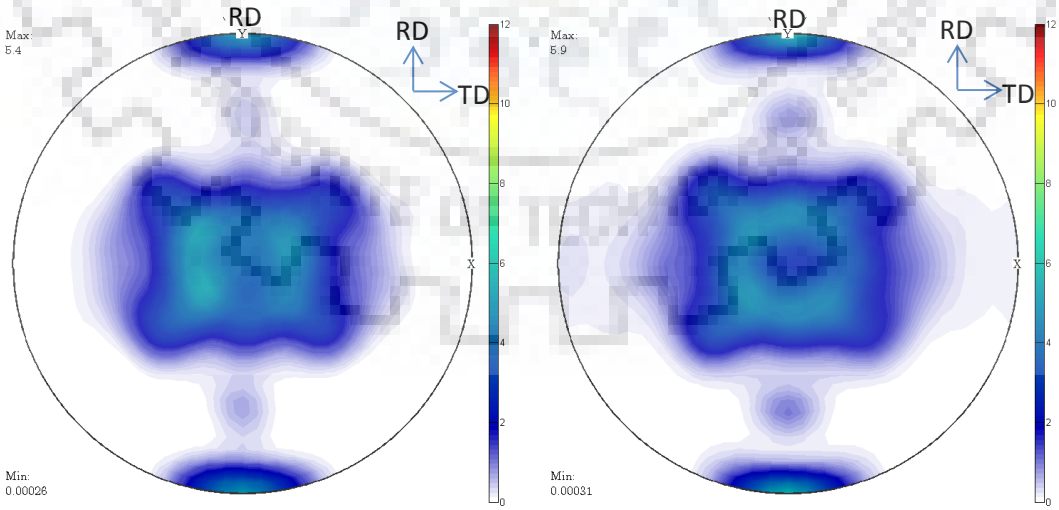

(a) 0.5 mm deformation (b) 1 mm deformation

Fig. 67: Pole Figure for (0002) Plane of WQ 900 Sample

Nano-Indentation : The nano-indentation for the WQ890 Sample was done which had both lamellar as well as equiaxed regions in order to know the nature of hardness and Young's modulus for the sample. The indents were made 50 in number in a grid of 5 × 10. The grid along with the hardness values and modulus values is obtained as follows :

Table 12: Young's Modulus (GPa)

145.12	147.13	127.11	140.94	134.68
142.16	154.03	151.49	144.82	144.34
134.79	141.74	132.89	142.6	141.81
144.52	127.36	140.57	161.34	146.29
175.04	134.38	134.68	120.25	130.46
131.02	128.78	155.7	135.96	134.62
151.49	144.51	137.88	158.76	144.92
136.82	142.18	123.5	123.85	135.66
127.87	133.4	133.6	129.92	126.55
127.42	143.1	136.92	132.52	143.83

Table 13: Nano-Hardness (GPa)

4.74	5.61	3.73	4.33	4.77
4.45	5.8	5.99	4.82	5.13
3.99	4.32	3.99	3.82	4.97
4.99	3.39	4.72	6.09	4.99
7.31	4.54	4.06	3.22	4.26
4.14	4.18	5.69	4.83	4.5
5.75	4.9	4.94	5.81	5.49
4.74	4.83	3.7	3.83	4.29
4.09	4.15	4.24	4.07	3.63
3.84	4.6	4.62	3.83	4.41

The average value of Young's modulus for the grid (Table 12) is 139.23 GPa whereas the average value of hardness from grid (Table 13) is 4.62 GPa. The standard deviation for the values of Young's modulus and hardness is 10.61 GPa and 0.794 GPa respectively. The average value of Young's modulus of these acicular martensites is 158.264 GPa whereas that for the equiaxed structure stands at 136.127 GPa. Similarly, for the Hardness values, the average value for hardness in case of predicted acicular morphology is at 5.86 GPa whereas for the equiaxed morphology, it is 4.3 GPa.

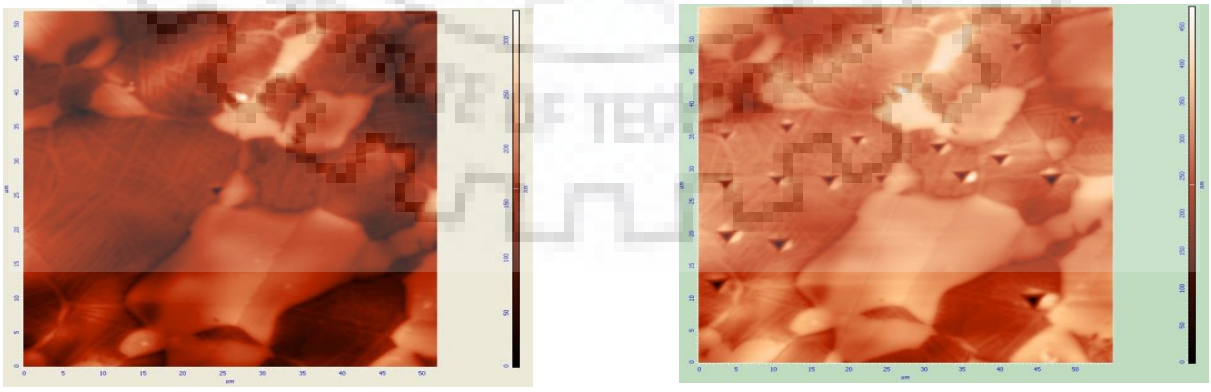

Fig. 68: Nano-Indentations on the WQ890 Sample

6.0 Summary

The project can be summarized as a way to generate a microstructure with lamellae forming within equiaxed morphology. The equiaxed morpohology was done using deformation followed by heat treatment, whereas martensite was formed in different fractions by quenching. The formation of martensite within this equiaxed morphology was then characterized using EBSD and S-XRD. The mechanical properties pertaining to obtained microstructure were characterized using tensile tests and nnao-indentation.

7.0 Conclusion

1. Microstructure with different fractions of martensite were generated.
2. However, the texture of α phase weaken with the martensite formation. Weakening of texture could enhance the ductility.

8.0 Scope for Future Work

The scope for future includes hot rolling at different temperatures so as to study the effect of deformation temperature on the globularization kinetics. Apart from this, there exists a vast field of texture upon which work can be expanded using the results of synchrotron x ray diffraction. The TEM studies also needs to be done in order to understand the martensite and the variants of martensite.

9.0 References

[1] M. Peters, J. Kumpfert, C. H. Ward and C. Leyens, "Titanium Alloys for Aerospace Applications," *Advanced Engineering Materials,* vol. 5, no. 6, pp. 419-427, 2003.

[2] J. C. Williams and E. A. Starke, "Progress in structural materials for aerospace systems," vol. 51, 2003.

[3] G. Lutjering and J. C. Williams, Titanium, Springer, 2007.

[4] D. J. Fernandes, C. N. Elias and R. Z. Valiev, "Properties and Performance of Ultrafine Grained Titanium for Biomedical Applications," *Materials Research*, vol. 18, no. 6, pp. 1163-1175, 2015.

[5] F. H. Froes, Titanium - Physical Metallurgy Processing and Applications, Ohio: ASM International, 2015.

[6] C. Leyens and M. Peters, Titanium and Titanium Alloys - Fundamentals and Applications, Weinheim: Wiley, 2003.

[7] H. Matsumoto, S. H. Lee, Y. Ono, Y. Li and A. Chiba, "Formation of Ultrafine-Grained Microstructure of Ti–6Al–4V Alloy by Hot Deformation of α' Martensite Starting Microstructure," *Advanced Engineering Materials,* vol. 13, pp. 470-474, 2011.

[8] R. Wanhill and S. Barter, "Metallurgy and Microstructure," in *Fatigue of Beta Processed and Beta Heat Treated Titanium Alloys*, Springer, 2012, pp. 5-10.

[9] D. J. Sheed, B. P. Kashyap and R. P. Singh, "Study of globularization in Ti-6Al-4V alloy during non-isothermal multiple forging and annealing," in *TheIIER International Conference*, London, 2015.

[10] S. A. A. Shams, S. Miramadi, S. M. Abbasi, D. Kim and C. S. Lee, "Mechanism of Martensitic to Equiaxed Microstructure Evolution during Hot Deformation of a Near-Alpha Ti Alloy," *Metallurgical and Materials Transactions A* , vol. 48A, pp. 2979-2992, 2017.

[11] H. Matsumoto, H. Yoneda, K. Sato, S. Kuroso, E. Maire, D. Fabregue, T. J. Konno and A. Chiba, "Room Temperature ductility of Ti-6Al-4V alloy with α' martensite microstructure," *Materials Science and Engineering A,* vol. 528, pp. 1512-1520, 2011.

[12] Y. Fan, W. Tian, Y. Guo, Z. Sun and J. Xu, "Relationships among the Microstructure, Mechanical Properties, and Fatigue Behavior in Thin Ti6Al4V," *Advances in Materials Science and Engineering,* 2016.

[13] H. Beladi, Q. Chao and G. S. Rohrer, "Variant selection and intervariant crystallographic planes distribution in martensite in a Ti–6Al–4V alloy," *Acta Materialia,* vol. 80, pp. 478-489, 2014.

[14] R. Pederson, "Microstrucutre and Phase Transformation of Ti-6Al-4V," Lulea Institute of Technology, Lulea, 2002.

[15] S. Zherebtsov, M. Murzinova, G. Salischev and S. L. Semiatin, "Spheroidization of the lamellar structure in Ti-6Al-4V alloy during warm deformation and annealing," *Acta Materialia,* vol. 59, pp. 4138-4150, 2011.

[16] H. Matsumoto, L. Bin, S. H. Lee, Y. Li, Y. Ono and A. Chiba, "Frequent Occurence of Discontinous Dynamic Recrystallization in Ti-6Al-4V Alloy with α' Martensite Starting Microstructure," *Metallurgical and Materials Transactions A ,* vol. 44A, pp. 3245-3260, 2013.

[17] Z. X. Zhang, S. J. Qu, A. H. Feng, J. Shen and D. L. Chen, "Hot Deformation Behavior of Ti-6Al-4V alloy : Effect of Initial Microstructure," *Journal of Alloys and Compounds,* vol. 718, pp. 170-181, 2017.

[18] S. M. Abbasi and A. Momeni, "Effect of hot working and post deformation on microstructure and tensile properties of Ti-6Al-4V," *Transactions of Nonferrous Metals Society of China,* vol. 21, pp. 1728-1734, 2011.

[19] N. Stanford and P. S. Bate, "The Martensitic Transformation Texture in Ti-6Al-4V," *Materials Science Forum,* Vols. 495-497, pp. 669-674, 2005.

[20] S. C. Wang, M. Aindow and M. J. Starink, "Effect of self-accommodation on a/a boundary populations in pure titanium," *Acta Materialia,* vol. 51, pp. 2485-2503, 2003.

[21] H. Wang, G. Sun, X. Wang, B. Chen, X. Zu, Y. Liu, L. Li, G. Pan, L. Sheng, Y. Liu and Y. Q. Fu, "In situ synchrotron X-ray diffraction analysis of deformation behaviour in Ti–Ni-based thin films," *Journal of Synchrotron Radiation,* vol. 22, pp. 34-41, 2015.

[22] I. Sen and U. Ramamurty, "Elastic modulus of Ti–6Al–4V–xB alloys with B up to 0.55 wt.%," *Scripta Materialia,* vol. 62, pp. 37-40, 2010.

[23] A. Kumar, U. Rabe and W. Arnold, "Mapping of Elastic Stiffness in an α+β Titanium alloy using Atomic Force Acoustic Microscopy," *Japanese Journal of Applied Physics,* vol. 47, no. 7, pp. 6077-6080, 2008.

[24] J. Cai, F. Li, T. Liu and B. Chen, "Investigation of mechanical behavior of quenched Ti-6Al-4V alloy by microindentation," *Materials Characterization,* vol. 62, pp. 287-293, 2011.

[25] J. L. W. Warwick, N. Jones, I. Bantounas, M. Preuss and D. Dye, "In situ observation of texture and microstructure evolution during rolling and globularization of Ti-6Al-4V," *Acta Materialia,* vol. 61, pp. 1603-1615, 2013.

[26] R. Srinivasan, M. D. Benett, T. Seshacharyulu, D. B. Miracle, K. O. Yu and F. Sun, "Rolling of Plates and Sheets from As-Cast Ti-6Al-4V-0.1B," *Journal of Materials Engineering and Performance,* vol. 18, pp. 390-398, 2009.

[27] S. L. Semiatin and T. R. Bieler, "The effect of alpha platelet thickness on plastic flow during hot working of Ti-6Al-4V with a transformed microstructure," *Acta Materialia,* vol. 49, pp. 3565-3573, 2001.

[28] S. L. Semiatin, V. Seetharaman and I. Weiss, "Flow behavior and globularization kinetics during hot working of Ti-6Al-4V with a colony alpha microstructure," *Materials Science and Engineering,* vol. A263, pp. 257-271, 1999.

[29] C. H. Park, K. T. Park, D. H. Shin and C. S. Lee, "Microstructural Mechanisms during Dynamic Globularization of Ti-6Al-4V alloy," *Materials Transactions,* vol. 49, pp. 2196-2200, 2008.

[30] H. Matsumoto, T. Nishihara, Y. Iwagaki, T. Shiraishi, Y. Ono and A. Chiba, "Microstructural evolution and deformation mode under high-temperature-tensile-deformation of the Ti-6Al-4V alloy with the metastable α′ martensite starting microstructure," *Materials Science and Engineering A,* vol. 661, pp. 68-78, 2016.

[31] A. D. Manshadi and R. J. Dippenaar, "Strain-induced phase transformation during thermo-mechanical processing of titanium alloys," *Materials Science and Engineering A: Structural Materials: Properties, Microstructure and Processing,* vol. 552, pp. 451-456, 2012.

[32] A. A. Salem, M. G. Glavicic and S. L. Semiatin, "The effect of preheat temperature and inter-pass reheating on microstructure and texture evolution during hot rolling of Ti–6Al–4V," *Materials Science and Engineering A,* vol. 496, pp. 169-176, 2008.

[33] T. Morita, K. Hatsuoka, T. Iizuka and K. Kawasaki, "Strengthening of Ti–6Al–4V Alloy by Short-Time Duplex Heat Treatment," *Materials Transaction,* vol. 46, no. 7, pp. 1681-1686, 2005.

[34] S. L. Semiatin , S. L. Kinsley, P. N. Fagin, F. Zhang and D. R. Barker, "Microstructure Evolution during Alpha-Beta Heat Treatment of Ti-6Al-4V," *Metallurgical and Materials Transactions A,* vol. 34A, pp. 2377-2386, 2003.

[35] G. C. Obasi, "Variant selection and its effect on texture in Ti-6Al-4V," University of Manchester, Manchester, 2011.

[36] Q. Chao, P. D. Hodgson and H. Beladi, "Ultrafine Grain Formation in a Ti-6Al-4V Alloy by Thermomechanical Processing of a Martensitic Microstructure," *Metallurgical and Materials Transactions A,* vol. 45A, pp. 2659-2671, 2014.

[37] M. Kuruvilla, T. S. Srivatsan, M. Petraroli and L. Park, "An investigation of microstructure, hardness, tensile behaviour of a titanium alloy: Role of orientation," *Sadhana,* vol. 33, no. 3, pp. 235-250, 2008.

[38] S. T. Oh, K. D. Woo, J. H. Kim and S. M. Kwak, "The Effect of Al and V on Microstructure and Transformation of β Phase during Solution Treatments of Cast Ti-6Al-4V Alloy," *Korean Journal of Metals and Materials,* vol. 55, no. 3, pp. 150-155, 2017.

[39] J. M. Manero, F. J. Gil and J. A. Planell, "Deformation mechanisms of Ti-6Al-4V alloy with a martensitic microstructure subjected to oligocyclic fatigue," *Acta Materialia,* vol. 48, pp. 3353-3359, 2000.